

ORIGINAL RESEARCH ARTICLE

Open Access



Optimal energy scheduling method for the North Cameroonian interconnected grid in response to load shedding

Bello-Pierre Ngoussandou¹, Nicodem Nisso², Dieudonné Kaoga Kidmo¹, E. Sreelatha³, Yosef Berhan Jember^{4*}, Sima Das⁵ and Kitmo^{1*} 

Abstract

Renewable energy sources like sun and wind are intermittent, hence a hybrid system incorporating them is necessary. However, certain systems are more cost-effective and efficient than others, and they are not only more expensive but also far more harmful to the environment. To make up for the energy shortage in unconnected remote regions and urban areas with linked networks, renewable energies offer an alternative. This effort is focused on eliminating both load shedding and the pollution caused by conventional power plants that burn fossil fuels. In order to improve the interconnected Northern Cameroon grid, researchers looked into the possibility of using the permanently accessible sun and wind at the Waibé-Lokoro-Kalfou location in Cameroon. For the hot and humid climate of Waibé-Lokoro, Cameroon, based on four distributed generations, four combinations were established in the scenario. The goal was to maximize the net present value while minimising the energy expense. Electricity costs were found to drop from USD 0.097/kWh to USD 0.085/kWh under the PV-Wind-Grid-Battery scenario, saving a total of USD 0.54 million in net present cost. The particle swarm optimization method (PSO), genetic algorithmic algorithm (GA), cuckoo search approaches (CSA), as well as whale optimization algorithm (WOA) were utilized to calculate power losses as well as system size allocation. PSO was the only algorithm to converge quickly. The level of distortion caused by harmonics is measured experimentally to verify that power grid connectivity regulations are being followed. The standards for the IEEE 33-bus as well as IEEE 69-bus tests provide more precise voltage profiles for use in loss evaluation.

Keywords Load shedding, Optimization, Hybrid system, Renewable energy sources

*Correspondence:

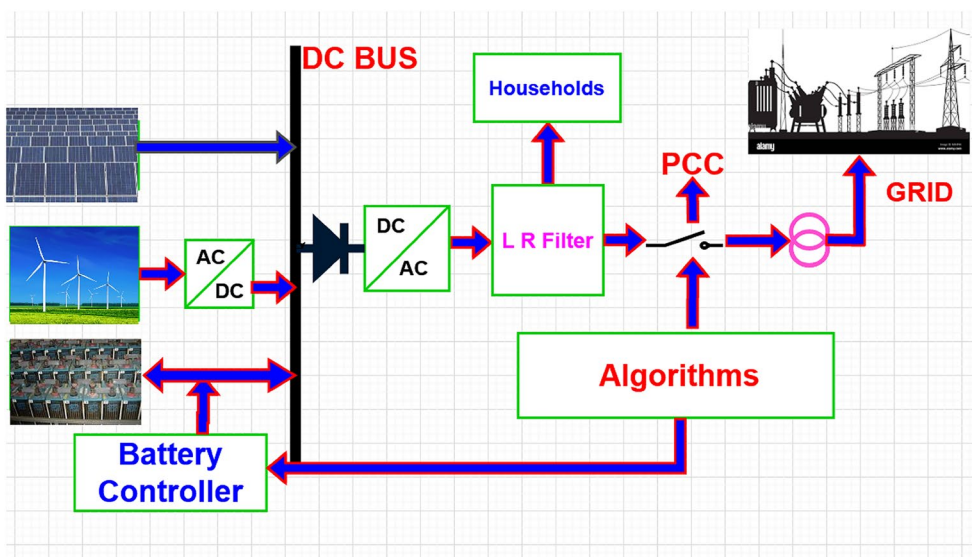
Yosef Berhan Jember
yosef.berhan@aait.edu.et
Kitmo
Kitmobahn@gmail.com

Full list of author information is available at the end of the article



© The Author(s) 2023. **Open Access** This article is licensed under a Creative Commons Attribution 4.0 International License, which permits use, sharing, adaptation, distribution and reproduction in any medium or format, as long as you give appropriate credit to the original author(s) and the source, provide a link to the Creative Commons licence, and indicate if changes were made. The images or other third party material in this article are included in the article's Creative Commons licence, unless indicated otherwise in a credit line to the material. If material is not included in the article's Creative Commons licence and your intended use is not permitted by statutory regulation or exceeds the permitted use, you will need to obtain permission directly from the copyright holder. To view a copy of this licence, visit <http://creativecommons.org/licenses/by/4.0/>.

Graphical Abstract



Introduction

For almost two decades, the number of households has increased due to the growing population in the northern part of Cameroon (Nsafon et al., 2020). This increase has led to a growing demand for electricity. As a result, there has been a low rate of access to electricity in households (especially in rural areas); in addition, there has been a drop in production at hydroelectric power stations due to unfavorable hydrology (as in the case of Lagdo, where the water level in the reservoirs has fallen and some turbines have stopped due to lack of maintenance) (Kitmo et al., 2021). When electrical installations are poorly dimensioned, equipment deteriorates as a result of overloading (there are considerable losses) (Jaszczur & Hassan, 2020). Another major problem is the impact of fossil fuels on the environment, leading to environmental pollution (water becomes toxic, acid rain destroys flora and fauna) (Sawle et al., 2017). Yet there is an abundance of non-polluting, non-degrading natural resources. Not only are these natural resources accessible to all, but their use does not lead to natural disasters such as flooding (Ram et al., 2022).

The sun is an appropriate source of electricity in rural areas and sunshine in the northern part of Cameroon is can produce between 5.74 and 6 kWh/m²/day. The work of Kidmo et al. (2015), shows that northern Cameroon has significant wind energy potential, which could provide an alternative to dependence on compromising energy.

However, the Northern Interconnected Network (NIN) has become almost obsolete due to load shedding (Bello-Pierre et al., 2023) and blackouts (Kitmo et al., 2021). In most of Cameroon’s ten regions, thermal power stations have been installed to back up the grid during blackouts. Some photovoltaic plants have been installed in localities such as Banjo, Guider and Tibati, but the power installed is small and cannot cover the needs of the population. Given this difficulty, it is important to find an urgent solution, which could involve combining renewable energy sources in isolated systems in rural areas and connected networks in urban areas (Yaouba et al., 2022). Unfortunately, isolated networks do not guarantee continuity of service. What’s more, knowledge and familiarity with these installations is still poor and almost non-existent. This is why solar installations are abandoned when they break down (Varma et al., 2012). As far as energy is concerned, it has not yet been used, even on an experimental basis, in the northern part of Cameroon. Some of the reasons for this are the high cost of production. However, many of the parameters surrounding the production of an energy should be taken into account to effectively assess whether certain statements are not flawed, or to see whether there are other similar solutions. Finally, once the power plant has been modelled, it could be combined with a photovoltaic power plant, which (Kitmo et al., 2022) research is presenting as an ideal solution for electrification in Cameroon.

Over the past few decades, demand for electricity has been growing as natural resources have been depleted (Al-Ghussain et al., 2021). This depletion is a consequence of climate change due to the deterioration of our universe by greenhouse gases produced by power plants such as nuclear and oil-fired power stations. Over time, resources such as uranium used in nuclear, coal and gas-fired power plants will no longer be sufficient to satisfy the world's needs by 2050 (Das et al., 2022). Moreover, the use of these resources exposes the world to environmental pollution from the carbon dioxide CO₂ produced during processing (Lin et al., 2021). Waste from the processing of non-renewable resources creates the global warming responsible for floods and deserts. Renewable energies hold great promise (Nsafon et al., 2020). Green energies offer an alternative to the problem of depleting natural resources. Having recognized these advantages, many countries are now proceeding to combine natural resources (renewable energies) to guarantee continuity of service and availability of energy in the face of growing demand for electricity in several countries, and even on certain continents, using multi-source power plants or hybrid systems (Djidimbélé et al., 2022). Decentralized renewable energy production is referred to as distributed generation (Alphonse et al., 2021), and is essentially owned by third parties. Distributed generation can be grouped into two main categories: decentralized generation, where the power supplier owns the grid and consumes its own energy (Tchaya et al., 2021). The energy is sold to the national sector, which owns the country's electrification system. This energy can also be sold to private individuals, or even to certain companies when there is sufficient surplus energy. The only condition governing this transaction is compliance with the IEEE 519 standard, which imposes a harmonic distortion rate of less than 5% before injection into the national grid at the common point of coupling (PCC) (Kitmo et al., 2021; Olivares et al., 2014). At the common coupling point or distribution connection point, two electricity meters are installed for billing surplus energy that is injected externally (Kavadias & Triantafyllou, 2021), and for inputting energy to the decentralized producer in the event of an energy deficit due to the lack of availability of its production resources (Schulz et al., 2021).

Then there's centralized generation. Under this system, the supplier of electrical energy is also the owner of the national electrification network. In Cameroon, for example, the national electrification network is called ENEO (Dieudonne et al., 2022). In this work, we look at the two aspects of renewable energy production in order to meet energy demand on the entire North interconnected network, known as the RIN. The North Cameroon Interconnected Network (NCIN) is made up of different feeders:

Adamaoua, North and Far North. These different sources are fed by the only source of hydroelectricity constituted, called the Lagdo hydroelectric dam located in the North region of Cameroon (Kitmo et al., 2021).

In Cameroon, photovoltaic solar energy is the second most widely used renewable energy after hydropower. It is most widely used in isolated areas of the country. Many studies on the challenges of renewable energies and the advantages of using them have encouraged the transformation of non-renewable energies into renewable energies. The hydroelectricity sector is the one that has been established in Cameroon since the first dams were built in the colonial years, in 1982. (Kitmo et al., 2021) estimate that the North Cameroon region has a significant wind energy potential compared with the other two regions of the septentrion, but their work is limited to assessing the potential in the far north of Cameroon, without taking into account a plan for the installation of hybrid sources to reinforce the northern interconnected network (NIN).

For over 15 years, the electricity sector has been experiencing serious problems (Yaouba, 2022). This problem has several causes: the first is population growth, and the second is the deterioration of the generation system. In addition, there is the problem of insufficient water to run the hydraulic turbines. The water tanks that should contain the volume needed to turn the turbines are completely and partially filled with sand. This is the case at the Lagdo hydroelectric power station. This has created a sense of urgency, as the population has been growing over the years, while electrical power has been decreasing exponentially.

Thermal power stations were installed in all 10 regions of Cameroon to meet the growing demand for energy. These are complemented by solar power plants in more isolated locations, such as Tibati and Banyo. In 2022, the grid-connected photovoltaic solar power plant in Guider, in the North Cameroon region, got a new lease of life. Thermal power plants produce carbon dioxide (CO₂), which is responsible for the greenhouse effect. On the other hand, fuel oil resources are not available, nor is coal for thermal power plants. In recent years, this has led to load shedding in almost all of Cameroon's ten regions.

The search for a solution to Cameroon's energy demand has so far been limited by the fact that the country's various back-up systems are unable to meet the growing demand for energy from its ever-changing population.

The work of Dieudonne et al. (2022) shows that it is possible to install wind power plants in Cameroon, especially in the northern part of the country. (Zieba Falama et al., 2022) evaluated the wind energy potential in the Adamoua, Nord and Far Nord regions. These studies showed that wind energy is abundant in the Guider

locality, where the average wind speed is 5 m/s during the months of March, April and May. Similarly, in Tcholliré, there is sufficient wind energy. However, these months correspond to the period during which several localities are constantly in the dark due to the lack of electrical energy produced by the Lagdo hydroelectric power station. Unfortunately, these works were limited to assessment. Added to this is the problem of maintenance and ageing power electronics equipment. Moreover, NASA climate data clearly show that an assessment of the photovoltaic solar deposit in the Guider locality could enable the reinforcement of the North Interconnected Grid line, which could be an alternative to the depletion of energy resources (Tonsie Djiela et al., 2020). On the basis of this work, it is now possible to think of a fusion of renewable sources, namely hydroelectric dams, solar photovoltaic generators and wind farms, to achieve the level of energy required by the various localities in the northern part of Cameroon (Manjong et al., 2021).

To meet energy demand, we also need to be aware of the problems posed by renewable energy installations. The use of wind power, for example, causes many problems of harmonic distortion. This is because the signals generated (current, voltage, power) contain continuous quantities. Wind power is an abundant source of harmonic distortion (Oliveira et al., 2017). This distortion creates phase imbalance. This distortion problem is compounded by Joule effect losses, conduction losses and switching losses due to the presence of power electronics components in the power generation system. More often than not, the electrical energy production system is inefficient and does not achieve the expected duration, due to the fact that the installation is poorly dimensioned on the one hand, and when the switching means for managing the communication sources are inadequate on the other (Tamalouzt et al., 2021). This is why research into algorithms (Balan, 2022) such as particle swarm optimization (Garg, 2016), genetic algorithms, fuzzy logic, neural networks, whale swarm optimization and mouse swarm optimization are essential for reducing power losses and increasing the efficiency of electrical installations. These methods (Shanmugam et al., 2022) can also be used to evaluate the size of electrical installations and the connection nodes or buses where distributed generation should be installed, in order to avoid line phase shifting (Alturki & Awwad, 2021).

Harmonics in PV/wind/hydro power systems originate in two ways (Lujano-Rojas et al., 2012): those injected into the system by non-linear loads such as incandescent lamps, televisions, microwave ovens and dishwashers. In addition, the harmonics generated by the system in the power grid feeding loads ahead of the common coupling point.

In addition, the power factor of the plant needs to be corrected, harmonics generated by the plant need to be reduced, and the hybrid system connected to the electrical grid needs to be sized in order to reduce the cost of installation and increase the service life of components. A major concern when using multi-source power plants is the quality of the energy produced. This is because decentralized producers must comply with the IEEE 519 standard, which imposes a voltage spill rate of 5% (Mahmoud, 2022) and a current spill rate of 3% for the injection of decentralized sources into power grids. The policy of decentralized production offers the possibility of purchasing green energy to compensate for a national electricity grid, and of reducing the greenhouse gases responsible for environmental pollution and the destruction of the ozone layer.

In reality, the use of renewable energies is a solution to compensate for the energy deficit on the northern interconnected grid (Kitmo et al., 2021). The prospect of integrating multi-source photovoltaic and wind power plants with hydroelectric power plants is a solution to the problem of load shedding or blackouts in the event of phase faults or plant maintenance requirements. And to solve the problem of harmonic distortion, active filters are better suited to cleaning up electrical installations. Unfortunately, the presence of passive dipoles always leads to system overheating and short-circuits.

In addition, the inclusion of mass density as a fixed variable makes it possible to standardize the manufacture of wind turbines. In terms of multi-source system optimization, maximum power point tracking can be used to improve the efficiency of hybrid photovoltaic/wind turbine systems (Mokhtara et al., 2021).

Therefore, the stochastic nature of energy due to random population growth makes it difficult to manage electrical energy. The design of multi-source installations does not take population growth into account. And once the population increases, these installations no longer supply the subscribed or expected power. The result is partial or total destruction of these installations due to overheating of the cables and receivers located on them. In some localities, solar photovoltaic installations are abandoned due to deterioration of the equipment before the expected duration, which demonstrates a huge loss because the cost of production is not amortized. Hence the need to find a suitable sizing method. Ma et al., (2021) proposed a PSO algorithm as a partial answer to solve these complexities. As the population grows, so should the number of solar panels. Unfortunately, existing systems do not guarantee the possibility of integrating other modules such as solar panels, inverters, batteries or turbines after the installations have been set up.

The use of conventional active filtering does not guarantee considerable suppression of harmonics. As a result, there are always switch delays, Joule effect losses and conduction losses. The same applies to the loss of synchronism after the hybrid system is hooked up to the electrical networks.

The manufacturers of wind turbines do not take into account the variation in mass density from one locality to another when extrapolating the power output of a wind power plant from datasheets, yet based on the law of variation in molar mass, each locality should have its own specific parameter. And we can't provide these data, which vary according to altitude or location for each part of the earth. This explains why the power output of wind turbines set by manufacturers is not always the power actually produced. As soon as you move from one location to another, the nominal parameters of wind turbines change, resulting in poor efficiency. In addition, one of the major problems faced by wind power plants is the distance to the grid interconnection site. Hence the need to look for sites close to hydroelectric power stations or interconnection substations.

Finally, the useful power given by solar panel manufacturers does not correspond to the power produced in the field. Solar panels lose their characteristics when subjected to climatic changes: temperature and solar radiation.

Geographical location of the Lokoro site

In addition to its abundant hydrocarbon resources, Cameroon's location in the region known as the Sahel gives it a prime spot for solar energy generation. Since the northern half of Cameroon is closer to the solar equator, it benefits from more sunlight than the southern parts of the country. The country's relatively flat landscape makes optimum use of the winds's average speed, making wind power the country's second most abundant resource. If current data is any indicator, an island nation's energy mix will benefit greatly from adding renewable sources like photovoltaic (PV) solar energy and wind power. Photovoltaic systems that are grid-connected have already demonstrated their economic value and ability to meet the grid's electricity needs. Extending power lines to extremely rural locations could not be cost-effective (Amigue et al., 2021). An alternative to costly network expansion is micro-electrical distributed central stations, as proposed by Njoh et al. (2019). However, the eolian systems studied in Hermann et al. (2021) thrive in the Arctic. In addition, (Muh et al., 2018) has designed, modeled, and constructed a 1.5 kilowatt (kW) experimental solar energy conversion system employing direct current (DC) motors with a maximum point of power tracking (MPPT) relation.

In the midst of the desert, there is a huge area known as Lokoro that measures 300.368 square kilometers. It was picked as an instance study because of the great potential it has for wind and solar energy. The climate of Lokoro

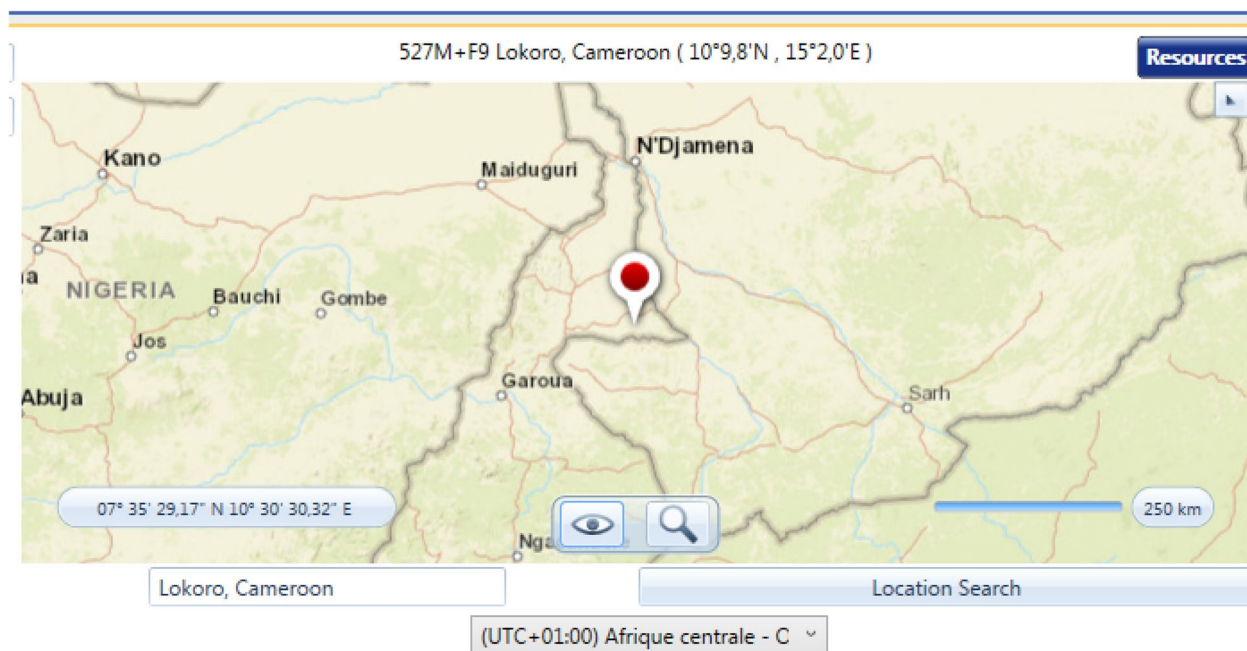


Fig. 1 Selected of Lokoro Area

Table 1 Solar irradiation data

Months	H (kW h/m ²)	T _{max} (Celsius)	Rh (percentage)
January	5.46	23.8	37
February	4.69	25.5	28
March	5.74	26.02	26
April	6.23	33.4	15
May	8.7	38.8	13
Jun	7.2	45.01	12
July	8.58	46.55	9
August	7.86	44.24	14
September	7.26	39.83	16
October	6.58	41.75	11
November	5.33	19.58	34
December	3.36	31.38	44
Mean Monthly	7.25	29.09	23.5

is dry and Sahelian (Gormo et al., 2021). The highest point in Lokoro is only 535 m above sea level, making for a fairly flat environment. Figure 1 depicts the case study area's physical location. Renewable energy sources, such as sun and wind, can be difficult to harness due to their unpredictability. This is due to the fact that maintaining a steady and trustworthy supply might be challenging. This is especially challenging in interconnected systems, where fluctuations in electricity generation from sources like solar and wind power must be managed, especially for smaller networks. Combining solar photovoltaics and wind power, for example, is a potential hybrid system that creates renewable energy at a low cost and with high reliability. The purpose of this article is to examine the process of developing, modeling, and implementing PI-optimized regulators for a grid-connected photovoltaic-electronic hybrid system (Donatus Iweh & Marius, 2019). An innovative particle swarm optimization, also known as the PSO method can be used to fine-tune the PI controller's gain settings. The proposed system was evaluated at two high-traffic times of the year to determine its potential effect on the overall network. Hourly mean climate information from the past decade was used to model the system. The system was finally analyzed economically and ecologically using the software Homer (Come Zebra et al., 2021).

Figure 1 shows the geographical location of the Lokoro locality where meteorological and spatio-temporal data are processed and analyzed.

Methods and materials location evaluation and resource selection

Table 1 shows monthly averages for worldwide horizontal irradiance, maximum temperatures, and humidity.

Lokoro meteorological data forecast

The information on radiation from the sun, wind speed, and temperatures was gathered from the ASECNA, the Organization for Aerial Flight Safety in Africa including Madagascar. From 2002 to 2022, the sample represents a median of the past decade. Based on these statistics, the software estimates an 11 percent inaccuracy for normal direct irradiance during the winter and spring months. In general, February and October have less sunlight than the rest of the year. Similar trends are shown in the average monthly amounts of both direct and indirect global horizontal radiation, with the maximum values occurring in June and July of each summer. Solar power systems that take into consideration tall wind turbines benefit most from May's moderate average monthly wind velocity of roughly 6 m per second, with a maximum speed of approximately 16.5 m per second. Most solar energy is produced during the summer and spring months. The average monthly temperature exhibits a clear upward trend over the summer, peaking at 37.5 °C in July. Photovoltaic generator efficiency would drop in winter, but the associated expenses and advantages would be substantially higher in summer, spring, and fall. The software has an inaccuracy of 35 Celsius degrees when reporting the temperature.

Systematical planning and parameter establishment

Lokoro's capacity for manufacturing and energy potential are used to size the system, while predicted performance as well as investment return are taken into account during the design phase. The size of the system guarantees that it can supply at least half of Lokoro's peak demand, and expanding its capacity would turn out to be financially impractical due to the hefty initial investment and the enormous amount of land that would be needed. There are many negatives to this, such as the fact that it will take a long time to remove dust from solar panels. The design also makes use of specialized topologies to maximize output power while minimizing waste and initial investment. PV Methodology. The PV generator has a 7 MW output and uses 15,330 panels, each of which has a 360 W nominal output. In order to increase power, the multi-string oscillator structure has been implemented. Five PV panel arrays are connected in series, and everyone has a DC-DC booster converter tied to an inverter. There are eight separate PV panels in each PV panel array. There are a total of 15,320 solar panels, 368 inverters to control 348 boost inverters, and 359 wires for transmission that make up the PV system. Each pair of panels in a chain faces south to maximize solar exposure

while minimizing land use, and there are three meters between adjacent pairs to prevent overshadowing.

An auxiliary transformer is needed to reduce the high voltage produced by the wind to the 16 kilovolts used by the connecting transmission lines. The total system's nominal power is 75 MW, however because to variations in radiation and wind, this is rarely achieved in practice. There's no denying the system will improve network performance and prevent blackouts even during high demand.

Solar energy system modelling

Four equations governing the solar generator's output current form the basis of the model (Meira Amaral da Luz et al., 2022):

$$\text{Photocurrent : } I_{ph} = [I_{sc} + k_i \cdot (T - T_n)] \cdot \frac{G}{1000} \quad (1)$$

$$\text{Saturation current : } I_0 = I_{rs} \cdot \left(\frac{T}{T_n}\right)^3 \cdot \exp\left[\frac{q \cdot E_{g0} \cdot \left(\frac{1}{T_n} - \frac{1}{T}\right)}{n \cdot K}\right] \quad (2)$$

$$\text{Reverse saturation current : } I_{rs} = \frac{I_{sc}}{\exp\left(\frac{q \cdot V_{oc}}{n \cdot N_s \cdot K \cdot T}\right) - 1} \quad (3)$$

$$\begin{aligned} \text{Output current : } I &= I_{ph} - I_0 \cdot \left[\exp\left(q \cdot \frac{(V + I \cdot R_s)}{n \cdot K \cdot N_s \cdot T}\right) - 1 \right] \\ &\quad - \frac{V + R_s \cdot I}{R_p} \end{aligned} \quad (4)$$

where I_{ph} , I_0 , I_{rs} , and I_{sc} represent photocurrent, semiconductor saturation, and inverse saturating, respectively. Current coefficients (k_i), temperature (T), nominal measurement temperature (T_n), electronic charge (q), and irradiance (G) are all represented by their respective symbols. In this article, we define some key characteristics of semiconductors, including the respective series as well as parallel resistance (R_s , R_p), the constant known as Boltzmann (K), the aggregate amount of parallel-connected cells in a given cell (N_s), and the electrical energy of the restricted band (E_{g0}). A the monocrystalline variety module panel is judged to have passed this test because of its extremely high manufacturing capacity of 18.04%, low price of roughly 0.5 \$/kW, and consistent performance in hot climates. Furthermore, contrary to common belief, monocrystalline solar cells function very well in dry climates. The panel's most salient features are detailed in

Table 2 Cell parameters

E_{g0}	Bandgap energy of the semiconductor (eV)	1.12
N_s	Number of cells connected in series	72
R_s	Series resistor (Ω)	0.100
R_p	Shunt resistor (Ω)	515
P_{max}	Maximum output power (W)	350
V_{mpp}	Maximum power voltage (V)	37.9
I_{mpp}	Maximum power current (A)	9.24

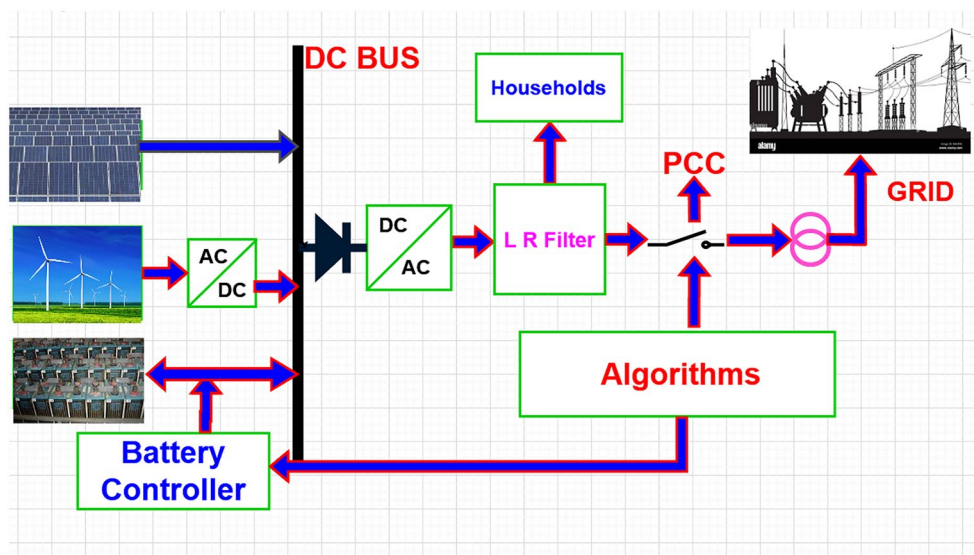


Fig. 2 Configuration of overall System

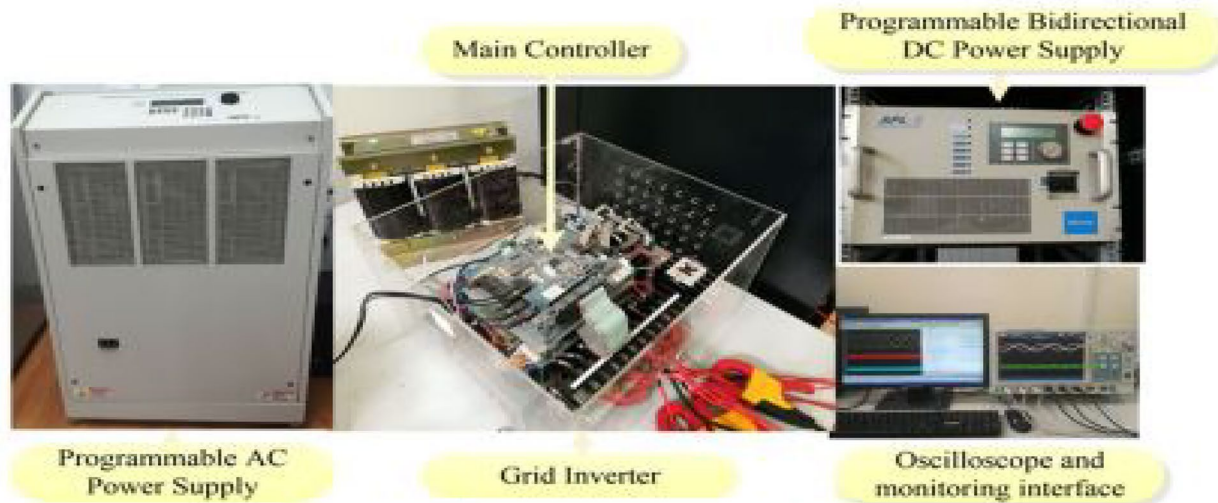


Fig. 3 Experimental Bench

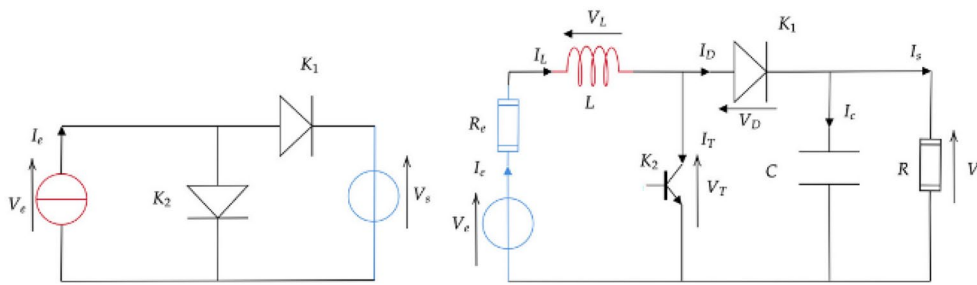


Fig. 4 DC converter and its current source

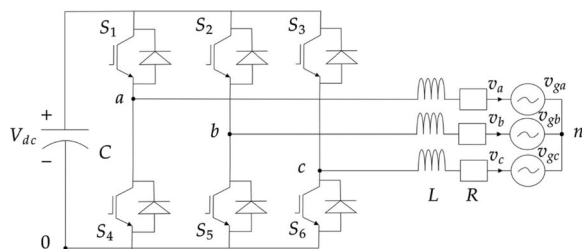


Fig. 5 DC-AC with LR filter configuration

converter. A LR filter depollutes the sources towards the common coupling point and protects the network from harmonics generated by the non-linear loads used by households. Thanks to the algorithms, energy is managed as a function of deficit and surplus at bus level.

Figure 3 shows the experimental bench used to evaluate the harmonic rate. The system is configured using an oscilloscope for curve display and a programmable controller.

Table 2. The formulae for determining series (R_s) and shunt (R_p) resistances are.

Figure 2 shows the overall system. The configuration of this system takes into account households and the interconnected network, which is that of the North Cameroon network. A photovoltaic generator, a wind farm and a battery bank are connected to a DC bus. The wind farm is connected to the DC bus via an AC-DC

DC to DC modelling

The output can be amplified by the CC converter amplifier, which is both efficient and robust. The PV generator’s variable CC outputs stress is fed into the converter, where it is transformed into a constant CC boosted tension. Figure 4 depicts the analogous electrical circuit, and Eqs. (1,2) are used to model the system (Jyothi et al., 2023).

$$\text{Loop 1 : } L \frac{di_L}{dt} = V_e - V_c(1 - \alpha) \tag{5}$$

$$\text{Loop 2 : } C \frac{dV_c}{dt} = i_L(1 - \alpha) - \frac{V_c}{R} \tag{6}$$

where a control the process of opening and reopening of the interrupter (K2) in the circuit, the PWM signal is generated via the MPPT’s cyclical relationship.

Transformer, three-phase

A voltage inverter links the PV array to the conventional power grid. The output of the converter supplies a constant voltage to the three-phase inverter in the elevator. The output of these inductors constitutes a pulse-width-modulated (PWM) set of three phases voltages (va, vb, and vc), and they are only utilized in high-power applications. Impulse width modulation is the process of adjusting the width of an impulse train in response to a relatively tiny control input. In Fig. 5, the RL filter (Kebbati & Baghli, 2023) is depicted as an integral part inside the electric oscillator circuit.

There are three reference frames that can be used to manage the three-phase inductors in Fig. 5:

the rotating synchronized connection frame (d-q), the reference frame that stays stationary (-), as well as the equilibrium reference frame (a-b-c). Triphasic electrical currents and voltages can be regulated by rotating the Park-type transformation inside the d-q basis reference in time with the stress in the network. Because of this, triangular variables expand indefinitely. Multiple filtering methods are available due to the continuous nature of the control variables. In addition, we’ll go into the specifics of how a brand-new PSO-PI was developed with the express goal of outperforming the control benchmark in question. These equations characterize the converter model:

$$a - b - c V_{k0} = L \frac{di_k}{dt} + Ri_k + V_{gk} + V_{n0} \tag{7}$$

$$V_{n0} = \frac{1}{3}(V_{a0} + V_{b0} + V_{c0}) \tag{8}$$

$$V_{k0} = S_k V_{dc} = \begin{cases} V_{dc} S_k = 1 \\ 0 S_k = 0 \end{cases} \tag{9}$$

where k is the phase relationship between the oscillators, S is the state of the upper commutators, and R is the serial resistance of the filter. The inductance of the filter is denoted by L, while the potential difference between ground and Vdc is written as Vn. We can write Eq. because we have absolute certainty that both circuit breakers will be functional during every oscillator phase.

Equation (19) summarizes the turbulent flow model, which takes into consideration mass in addition the forces affecting a, b, and c.

$$\begin{bmatrix} v_{a0} \\ v_{b0} \\ v_{c0} \end{bmatrix} [= \frac{V_{dc}}{2} \times \begin{bmatrix} S_a \\ S_b \\ S_c \end{bmatrix} \tag{10}$$

$$\begin{bmatrix} v_a \\ v_b \\ v_c \end{bmatrix} [= \frac{1}{3} \begin{bmatrix} 2 & -1 & -1 \\ -1 & 2 & -1 \\ -1 & -1 & 2 \end{bmatrix} \times \frac{V_{dc}}{2} \times \begin{bmatrix} S_a \\ S_b \\ S_c \end{bmatrix} \tag{11}$$

For Modulation control, the network’s tilt is determined by monitoring strains with a phase-locking loop (PLL). The PLL technique is extensively described. The Park transformation uses the grille angle to map the a-b-c component of the grille stresses to the d-q reference structure, simplifying the control and resulting in Vgd and Vgq. The oscillator’s output tensions are transformed in the same way to produce Vid et Viq (the elements of the d-q oscillator). A description of Park’s strategy has been:

$$\begin{bmatrix} V_d \\ V_q \end{bmatrix} = \frac{2}{3} \begin{bmatrix} \cos\theta & \cos(\theta - \frac{2\pi}{3}) & \cos(\theta - \frac{4\pi}{3}) \\ -\sin\theta & -\sin(\theta - \frac{2\pi}{3}) & -\sin(\theta - \frac{4\pi}{3}) \end{bmatrix} \begin{bmatrix} V_a \\ V_b \\ V_c \end{bmatrix} \tag{12}$$

RL filtering

Using a vectorial control strategy, a RL filter produces active as well as reactive powers that can be converted in d-q tension phase through the converter and the network (Kebbati & Baghli, 2023). These equations form the basis of the RL filter’s design in Fig. 5

$$a - b - c : V_a = -R_f.i_a - L_f \frac{di_a}{dt} + V_{ga} \tag{13}$$

$$V_b = -R_f.i_b - L_f \frac{di_b}{dt} + V_{gb} \tag{14}$$

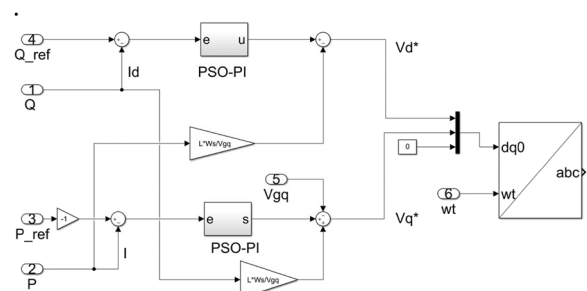


Fig. 6 System of PLL control

$$V_c = -R_f \cdot i_c - L_f \frac{di_c}{dt} + V_{gc} \tag{15}$$

$$d - qV_d = -R_f \cdot i_d - L_f \frac{di_d}{dt} + L_f \omega i_q + V_{gd} \tag{16}$$

$$V_q = -R_f \cdot i_q - L_f \frac{di_q}{dt} - L_f \omega i_d + V_{gq} \tag{17}$$

where L represents the filter’s inductance (Lf) and R stands for its resistance (Rf). The RL filter connects the inductance (Lf) and resistance (Rf) of the filter are denoted by the letters L and R, respectively. Because of their different impedances and phases, the RL filter creates a stress gap when connecting its inductive element with the electrical network. Additionally, it lessens electronic harmonics produced by the system. In order to prevent reactive power generation and guarantee a zero-degree phase mismatch between the supply voltage and the load current, active power is determined by comparing the observed reactive output (P*) to a reference value (Q*) equal zero. On the other side, the output of the PV generator determines P*. To fix the problems, the PSO-PI controller makes corrections to the d-q inverter’s reference voltages (Vd* and Vq*). Figure 5 depicts the discovery’s underlying mechanism, which consists of Vd* and Vq*.

To operate the motor’s interrupters, the resulting voltages are inverted using the Park transformation creating three-phase on-off-reference values (Va*, Vb*, and Vc*), which are subsequently contrasted to a running MATLAB sequence. Upper commutator state, represented by PWM signals, is specified by the Eq. (9). The Park transformation can be inverted by using the following equation, which is also known as the “d-q to a-b-c” transformation.

$$\begin{bmatrix} V_a \\ V_b \\ V_c \end{bmatrix} = \begin{bmatrix} \cos(\theta) & -\sin(\theta) \\ \cos(\theta - \frac{2\pi}{3}) & -\sin(\theta - \frac{2\pi}{3}) \\ \cos(\theta - \frac{4\pi}{3}) & -\sin(\theta - \frac{4\pi}{3}) \end{bmatrix} \begin{bmatrix} V_d \\ V_q \end{bmatrix} \tag{18}$$

Energy system modeling

The turbines, also known as wind plant, can be alternatively dynamic as well as mechanical in design, Electricity for the wind farm is generated by turbines, often called wind plants, which may be either mechanical or dynamic in construction and are linked to a pair of double-fed induction generators (or "multipliers"). Figure 6 shows that the DFIG stator is connected immediately to the network and is synchronized with it, while the rotor links to the network via two back-to-back converters that each

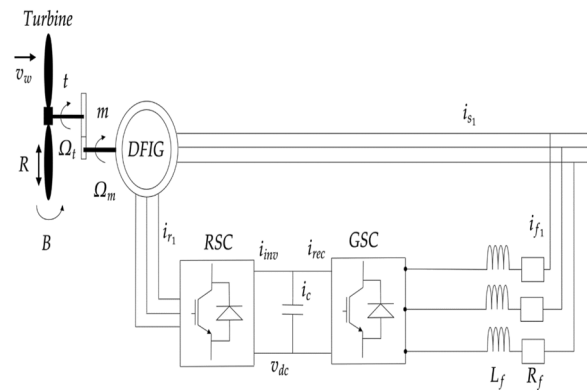


Fig. 7 Wind plant configuration

contain a correcting device, an inductive element used to power a bus, and a filter.

Wind power station dynamical model

Equation (19) describes the mechanical power gained from the wind (Kebbat & Baghli, 2023).

$$P_t = \frac{1}{2} \rho C_p(\varphi, \beta) \pi R^2 V^3 \tag{19}$$

TSR being defined as

$$\varphi = \frac{\Omega_t \cdot R}{V} \tag{20}$$

Cp and R stand for the power coefficient and the radius of the turbine blades, while stands for the density of the air. V denotes the velocity of the wind, Ω_t is the rotational speed of the turbine, and the angular tilt of the turbine. The maximum power coefficient depends on the values of and. To write down the highest possible power efficiency for a 7 MW wind, we have:

$$C_p = C_1 \times (C_2 \times \frac{1}{\varphi_i} - C_3 \times \beta - C_4) \times \exp(-\frac{C_5}{\varphi_i}) + C_6 \times \varphi \tag{21}$$

where

$$(\frac{1}{\varphi_i} = \frac{1}{\varphi + 0.08 \times \beta} - \frac{0.035}{\beta^3 + 1}) \tag{22}$$

Mechanical turbine model of wind

The speed (m) is calculated by comparing the generator and turbine temperatures (T_m and T_v, respectively). Classical rotational dynamics equation governs mechanical system behavior:

$$\left(\frac{J_t}{G^2} + J_m\right) \frac{d\Omega_m}{dt} + f_v \times \Omega_m = T_t - T_m \tag{23}$$

where J_t and J_m are the inertia moments of the turbine and alternator, and f_v is the friction coefficient of the alternator. MPPT controller for solar energy systems. The main points motor’s rotational speed is adjusted in relation to a reference pair using the highest feasible power point Tracking method to ensure maximum power extraction. In order to achieve the maximum power coefficient (C_{pmax}), it is crucial to maintain the TSR at its optimal value (opt). Maximum Power Point Tracking, also known as MPPT, and turbine supervision are depicted in Fig. 7.

Design of a dual-fuel induction generator

The DFIG takes inspiration from Park’s playbook to facilitate the anti-victory strategy’s deployment. The mutual inductive devices of both the rotor and the stator fluctuate a sinusoidal pattern as an estimate of the electric angle, but otherwise this model is a simplification of the one given in Kebbati and Baghli (2023) Stator as well as rotor voltages are regulated by the Park reference formulas (24–38).

$$V_{sd} = R_s \cdot i_{sd} + \frac{d\varphi_{sd}}{dt} - \dot{\theta}_s \cdot \varphi_{sq} \tag{24}$$

$$V_{sq} = R_s \cdot i_{sq} + \frac{d\varphi_{sq}}{dt} + \dot{\theta}_s \cdot \varphi_{sd} \tag{25}$$

$$V_{rd} = R_r \cdot i_{rd} + \frac{d\varphi_{rd}}{dt} - \dot{\theta}_r \cdot \varphi_{rq} \tag{26}$$

$$V_{rq} = R_r \cdot i_{rq} + \frac{d\varphi_{rq}}{dt} - \dot{\theta}_r \cdot \varphi_{rd} \tag{27}$$

where D-Q Tension (V_{sd} , V_{sq}), D-Q Current (I_{sd} , I_{sq}), D-Q Tension (V_{rd} , V_{rq}), and D-Q The current (I_{rd} , i_{rq}) all need to be specified. Rotor and stator d-q and d-r fluxes; rotor and stator resistances; radial and angular displacements of the rotor and stator; R_r and R_s . Stator as well as rotor flow d-q components are established by:

$$\varphi_{sd} = L_s \cdot i_{sd} + m \cdot L_m \cdot i_{rd} \tag{28}$$

$$\varphi_{sq} = L_s \cdot i_{sq} + m \cdot L_m \cdot i_{rq} \tag{29}$$

$$\varphi_{rd} = L_r \cdot i_{rd} + m \cdot L_m \cdot i_{sd} \tag{30}$$

$$\varphi_{rq} = L_r \cdot i_{rq} + m \cdot L_m \cdot i_{sq} \tag{31}$$

$$L_s = L_{fs} + L_m \tag{32}$$

$$L_r = L_{fr} + m^2 \cdot L_m \tag{33}$$

where the inductance of the stator (L_s), the rotor (L_r), and the magnet (L_m) are denoted by their respective symbols. L_{fs} and L_{fr} stand for the leakage inductances of the stator and rotor, whereas m represents the transformation ratio. Using the formulas (33–36), we can calculate the stator and rotor active and reactive powers.

$$P_s = V_{sd} \cdot i_{sd} + V_{sq} \cdot i_{sq} \tag{34}$$

$$P_r = V_{rd} \cdot i_{rd} + V_{rq} \cdot i_{rq} \tag{35}$$

$$Q_r = V_{rq} \cdot i_{rd} - V_{rd} \cdot i_{rq} \tag{36}$$

In Eq., T_m is the electromagnetic torque.

$$T_m = p \cdot (\varphi_{sd} \cdot i_{sq} - \varphi_{sq} \cdot i_{sd}) \tag{37}$$

$$T_m = p \cdot \frac{m \cdot L_m}{L_s} \cdot (\varphi_{sq} \cdot i_{rd} - \varphi_{sd} \cdot i_{rq}) \tag{38}$$

where p is the total amount of pole pairs.

DFIG control theory

In order to produce the reduced DFIG model used in the d-q reference, the winding of the stator resistance is disregarded.

$$V_{sd} = 0 \tag{39}$$

$$V_{sq} \text{istance} = U_s = \omega_s \cdot \varphi_{sd} \tag{40}$$

$$V_{rd} = R_r \cdot i_{rd} + \frac{d\varphi_{rd}}{dt} - \omega_r \cdot \varphi_{rq} \tag{41}$$

$$V_{rq} = R_r \cdot i_{rq} + \frac{d\varphi_{rq}}{dt} - \omega_r \cdot \varphi_{rd} \tag{42}$$

Through solving for the stator and rotor fluxes, we can calculate the stator currents as:

$$i_{sd} = \frac{\varphi_{sd} - m \cdot L_m \cdot i_{rd}}{L_s} \tag{43}$$

$$i_{sq} = -m \cdot \frac{L_m}{L_s} \cdot i_{rq} \tag{44}$$

This leads to the following form for the rotor flux equations:

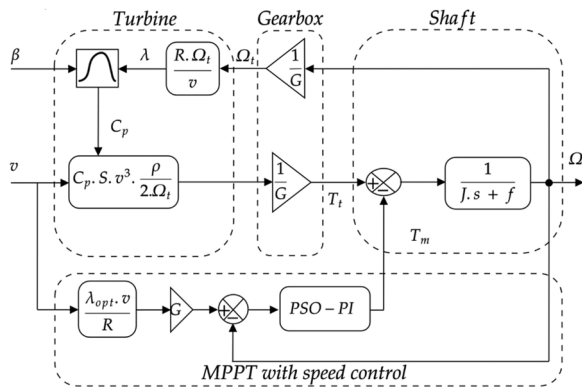


Fig. 8 DFIG control techniques

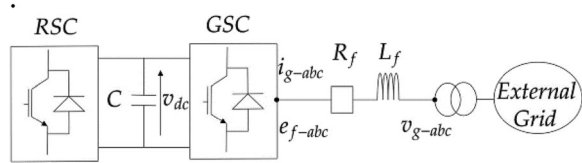


Fig. 9 Grid side control-based RL filter

$$\begin{aligned} \varphi_{rd} &= \left(L_r - \frac{(m \cdot L_m)^2}{L_s} \right) \cdot i_{rd} + m \cdot \frac{L_m}{L_s} \\ \varphi_{sd} &= \sigma \cdot L_r \cdot i_{rd} + m \cdot \frac{L_m}{L_s} \cdot \varphi_{sd} \end{aligned} \tag{45}$$

$$\varphi_{rq} = L_r \cdot i_{rq} - \frac{(m \cdot L_m)^2}{L_s} \cdot i_{rq} = \sigma \cdot L_r \cdot i_{rq} \tag{46}$$

For the leakage coefficient, let's write:

$$\sigma = 1 - \frac{(m \cdot L_m)}{L_s \cdot L_r} \tag{47}$$

The rotor fluxes are obtained by exchanging the impact of direct and quadrature components:

$$v_{rd} = R_r \cdot i_{rd} + \sigma \cdot L_r \frac{di_{rd}}{dt} + e_{rd} \tag{48}$$

$$v_{rq} = R_r \cdot i_{rq} + \sigma \cdot L_r \frac{di_{rq}}{dt} + e_{rq} + e_\varphi \tag{49}$$

where

$$e_{rd} = -\sigma \cdot L_r \cdot \omega_r \tag{50}$$

$$e_{rq} = \sigma \cdot L_r \cdot \omega_r \cdot i_{rd} \tag{51}$$

$$e_\varphi = \omega_r \cdot m \cdot \frac{L_m}{L_s} \cdot \varphi_{sd} \tag{52}$$

The electromagnetic torque becomes as follows:

$$T_m = -p \cdot \frac{m \cdot L_m}{L_s} \cdot \varphi_{sd} \cdot i_{rq} \tag{53}$$

Therefore, the equations below describe the reactive and active forces.

$$P_S = -v_{sq} \cdot m \cdot \frac{L_m}{L_s} \cdot i_{rq} \tag{54}$$

$$Q_S = \frac{v_{sq} \cdot \varphi_{sd}}{L_s} - v_{sq} \cdot m \cdot \frac{L_m}{L_s} \cdot i_{rd} \tag{55}$$

These formulae make it clear that selecting a d-q chassis makes the power output of the stator proportional to the q-component of the rotor's current, while the d-component has no bearing on the reactive power output. This means that the rotor's current d-q components can be used to regulate power without affecting the stator's active or reactive components. Reference d-q rotor currents are required for controlling d-q rotor current components. These values are calculated using the rotor's magnetic flux and the given formula:

$$\varphi_{sd-est} = L_s \cdot i_{sd} + m \cdot L_m \cdot i_{rd} \tag{56}$$

Then, the components of the reference's rotor current are created as follows:

$$i_{rq}^* = -\frac{L_s}{p \cdot m \cdot L_m \cdot \varphi_{sd-est}} \cdot T_m^* \tag{57}$$

$$i_{rd}^* = \frac{\varphi_{sd-est}}{m \cdot L_m} - \frac{L_s}{m \cdot L_m \cdot v_{sq}} \cdot Q_s^* \tag{58}$$

The DFIG's control mechanism, guaranteed through the rotor sides converter (RSC), is depicted in Fig. 8.

An output voltage-based modulation of pulse width (PWM) output regulates the converter's operation.

Inverter and filter that can connect to the grid

In order to control the reactive injection of electricity and bus CC voltage, the GSC is wired into the system via an RL filter, as shown in Fig. 9. It is assured that the single-factor power will be present when the reactive power of the system is zero (Q=0).

Grid-side circuit three-phase equations are given in Eqs.

$$v_{ga} = R_f \cdot i_{ga} + L_f \frac{di_{ga}}{dt} + e_{fa} \tag{59}$$

$$v_{gb} = R_f \cdot i_{gb} + L_f \frac{di_{gb}}{dt} + e_{fb} \tag{60}$$

$$v_{gc} = R_f \cdot i_{gc} + L_f \frac{di_{gc}}{dt} + e_{fc} \tag{61}$$

The d-q representation is obtained by translating the equations into the synchronized rotating frame, which yields the following:

$$v_{fd} = -R_f \cdot i_{fd} - L_f \frac{di_{fd}}{dt} + e_{fd} \tag{62}$$

$$v_{fq} = -R_f \cdot i_{fq} - L_f \frac{di_{fq}}{dt} - e_{fq} \tag{63}$$

where

$$e_{fd} = \omega_s \cdot L_f \cdot i_{fq} \tag{64}$$

$$e_{fq} = -\omega_s \cdot L_f \cdot i_{fd} + v_{gq} \tag{65}$$

Using the reference values i_{fd}^* and i_{fq}^* , the PSO-PI controller is able to independently adjust the RL filter currents using the GSC. The GSC's active and reactive powers are known to be supplied by:

$$P_f = V_{fd} \cdot I_{fd} + V_{fq} \cdot I_{fq} \tag{66}$$

$$Q_f = V_{fq} \cdot I_{fd} + V_{fd} \cdot I_{fq} \tag{67}$$

Since it is assumed that the stresses vector is vertical to the q-axis within the synchronously rotating frame, the resistance phase that makes up the RL filter can be disregarded when estimating the d-q component parts of the tension:

$$v_{sd} = 0, v_{sq} = \hat{v}_g.$$

Similar to how both active alongside reactive energies can be used as references, the reverse is also true:

$$P_f = V_{sq} \cdot I_{fq} \tag{68}$$

$$Q_f = V_{sq} \cdot I_{fd} \tag{69}$$

$$P_f^* = I_{fq}^* \cdot V_{sq} \tag{70}$$

$$Q_f^* = I_{fd}^* \cdot V_{sq}$$

The DC bus's power is subdivided into:

$$P_{RSC} = V_{dc} \cdot I_{RSC} \tag{71}$$

$$P_C = V_{dc} \cdot I_c \tag{71}$$

$$P_{GSC} = V_{dc} \cdot I_{GSC} \tag{73}$$

$$P_{RSC} = P_c + \text{Joule} \tag{74}$$

When power losses in the condenser are ignored, the voltage across the converters and the load line (RL) is equalized, and Pf control translates to Pc control, which in turn translates to Vdc control. As can be seen in Fig. 10 of the GSC Simulink model, the rotor's q-component current controls the CC-connection's voltage.

Controlling using PSO-PI

PI controllers are used extensively in industry because to their user-friendliness and dependability. Based on this error signal, the controller issues a directive according to the following equation:

$$u(t) = k_p e(t) + k_i \int e(t) dt \tag{75}$$

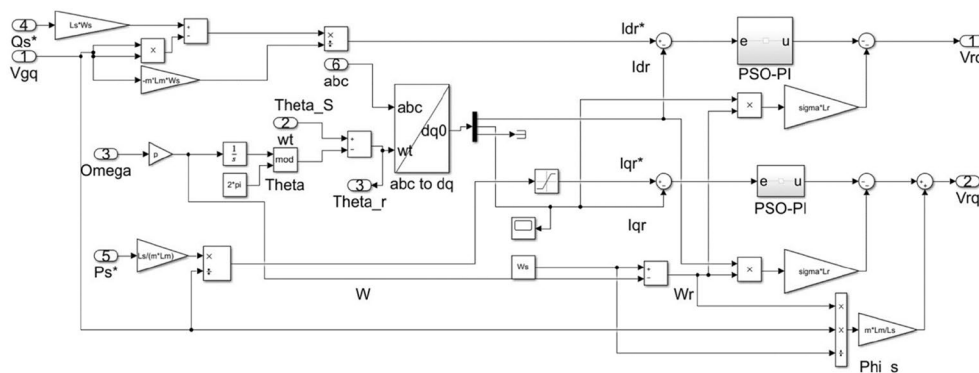


Fig. 10 Synchronization using Park transformation

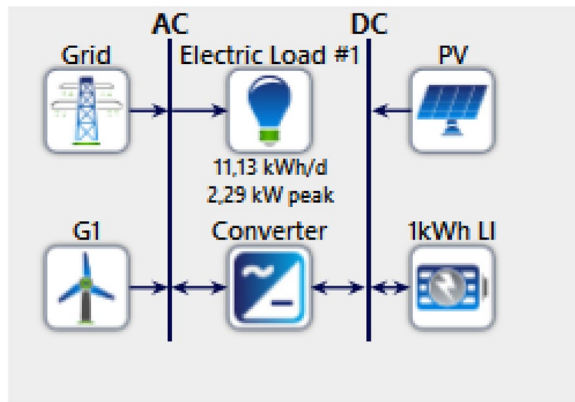


Fig. 12 System configuration using HOMER software

must incorporate not just the cost of the system but also transportation, packing, and set-up. The formula below can be used to calculate the amount spent on capital expenditures.

Use of the planning system HOMER

Homer (Kebbaty & Baghli, 2023) is used to analyze the financial and ecological impacts of fully connecting the system to the network. All of the generated electricity will be added to the regional distribution system. Homer is a tool that can calculate rough estimates of recurring expenses as those found in tech upkeep, repair, and replacement. Operating and maintenance costs include things like insurance premiums, salaries, taxes, and other periodic expenditures. They are presented as a percentage of the total seed money. Components of a system have replacement costs anytime they are updated due

to their varying degrees of dependability and the possibility of numerous replacements over the course of their service life. When doing economic evaluations, the leveling cost of energy (LCOE) is the most important factor to consider when assessing the profitability of energy systems. This final price takes into account all energy units produced by the components of the system over the course of its lifetime.

To determine the LCOE, we divide the total energy produced by the system from the sum that includes the LCOE and the costs of setup, operation, and upkeep. The discounted cash flow method can be used to determine the LCOE. The LCOE is calculated by dividing the total expenditures of the system by its total income.

$$LCOE = \frac{I_0 + \sum_{t=1}^n \frac{A_t}{(1+i)^t}}{\sum_{t=1}^n \frac{M_{t,el}}{(1+i)^t}} \tag{79}$$

where I_0 , A_t , and $M_{t,el}$ stand for the initial investment, annual cost, and production (in megawatt-hours), respectively. Interest rate per year (i), economic cycle length (n), and calendar year (t) are all indicated by their corresponding abbreviations. The VAN calculates the overall profit and true worth of the construction endeavor at any time by discounting the future benefit and expenditure flows to the present. The VAN is calculated by subtracting outgoing cash flows from incoming cash flows over a specified time frame. In order to determine a project's total cost, the VAN formula employs value equivalents.

$$NPV = \sum_{t=1}^n \frac{R_t - C_t}{(1+i)^t} - I_0 \tag{80}$$

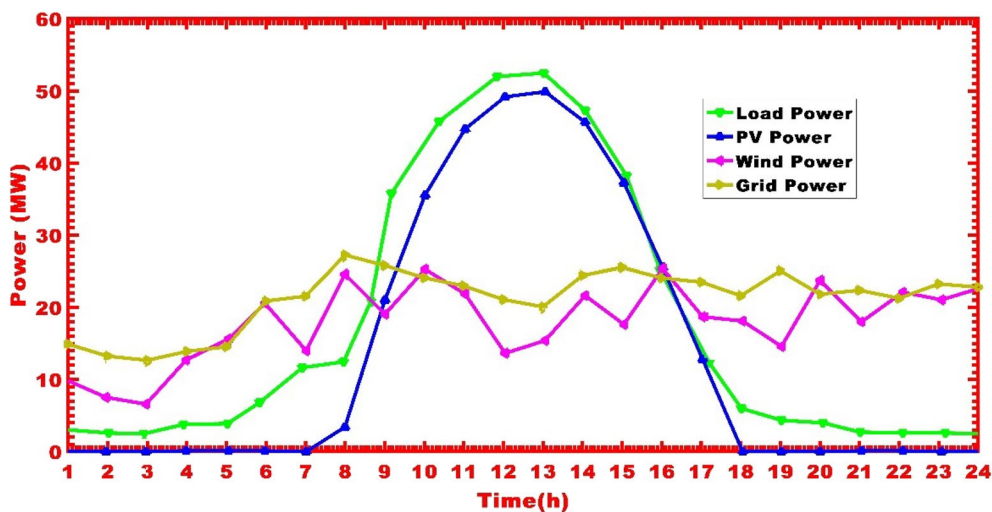


Fig. 13 Load Profile

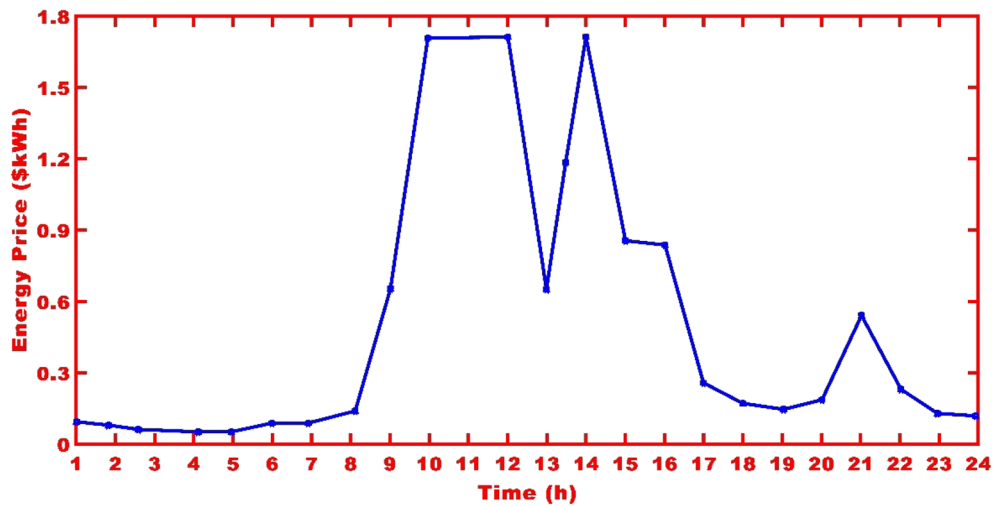


Fig. 14 System configuration using HOMER software

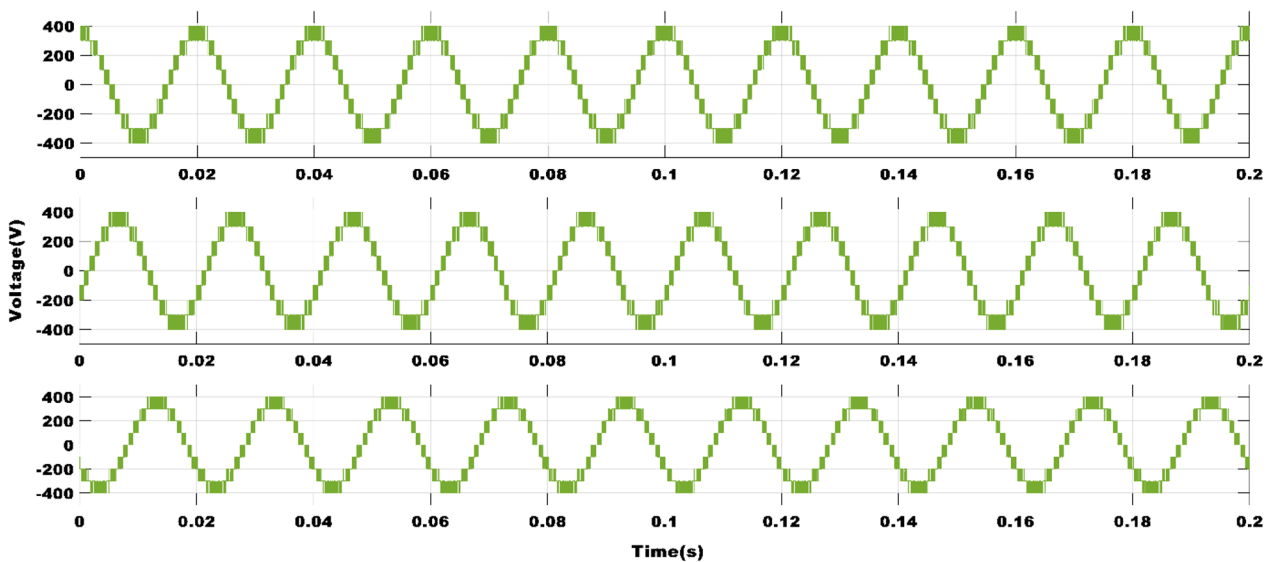


Fig. 15 Three phases inverter voltages

where R_t along with C_t are sales and costs in year t ; i is the compound annual growth rate; and I_0 is the initial investment. The time that it requires for a system to get its money back from the project in the form of cash flows is known as the recovery period. The faster you can repay your initial investment, the better. After the end of the recovery period, cash flow distribution are often planned. Below is a formula that can be used to approximate how long it will take to recover:

$$\text{Payback period} = \frac{\text{Initial Investment}}{\text{Cash inflow per period}} \quad (81)$$

Figure 12 shows the configuration of the overall system in the HOMER software. From this configuration we can see the different parts which make up the scenarios: PV-wind, PV-wind-battery, PV-wind-battery-grid. The cost evaluation of this overall system in HOMER gives an idea of the optimization or feasibility before the operations are implemented.

Results and discussion

Figure 13 shows the household load profile, the photovoltaic power, the wind power and the grid power profile. These power profiles are presented over a 24-h period with loads running at full capacity. An average of 35 MW

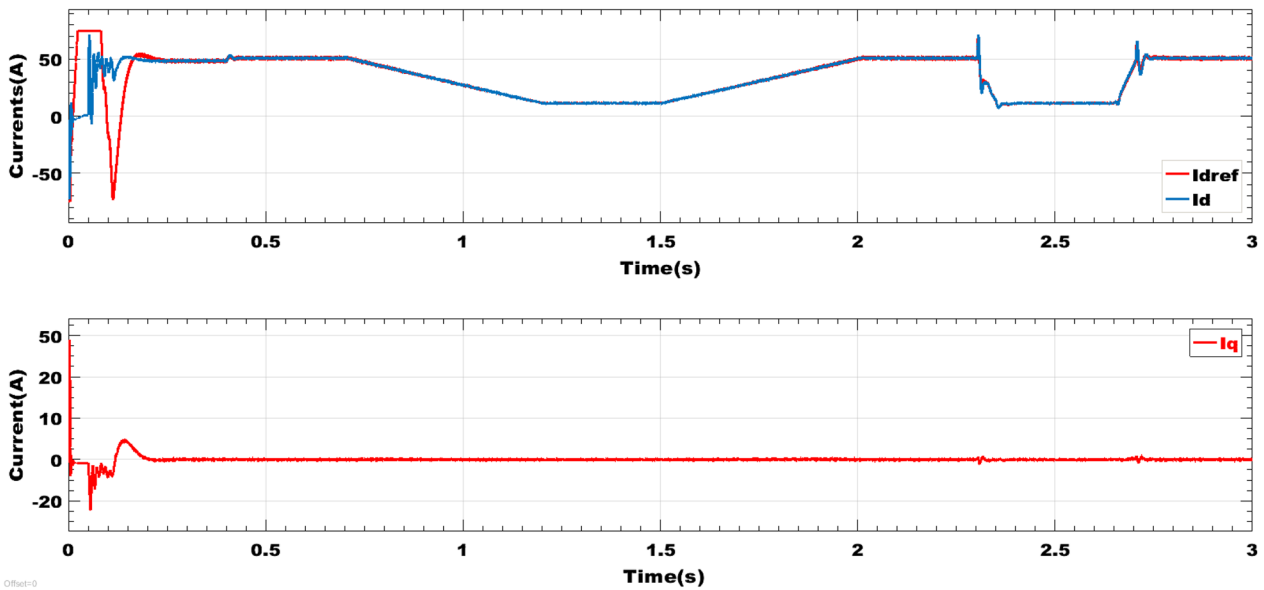


Fig. 16 System configuration using HOMER software

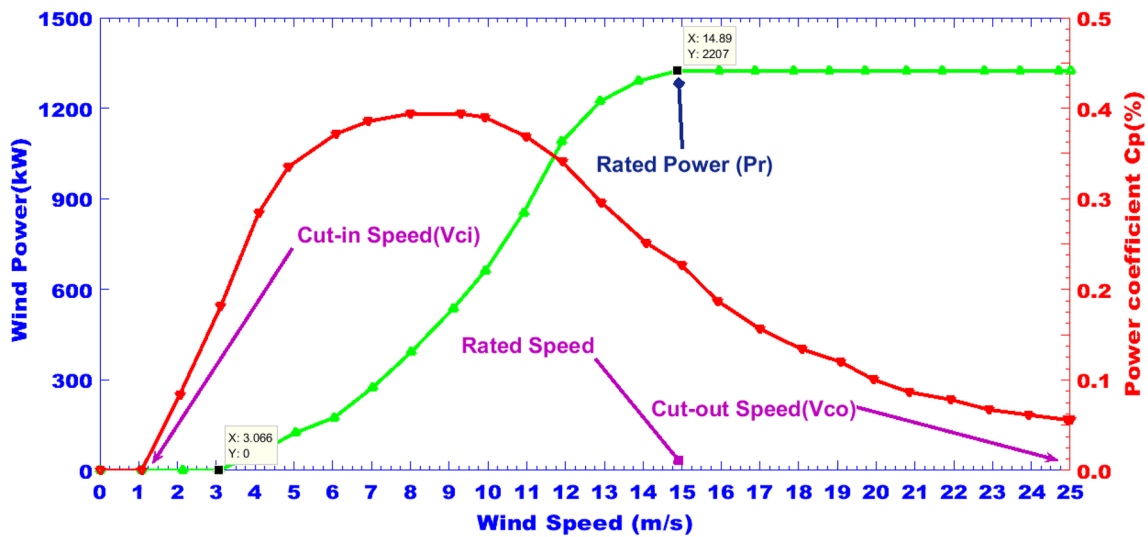


Fig. 17 DFIG pitch control

is available over a 24-h period thanks to the combination of different sources.

Figure 14 shows the cost of energy for an average day. From this curve we can see that the cost of producing energy evolves as a function of demand over a 24-h period. This figure shows that the cost of production has decreased considerably thanks to the algorithms chosen for this optimization.

Figure 15 shows the voltage profile of the inverter that is assumed to be connected before calculating the rate of harmonic distortion at the common coupling point

(PCC). Thanks to this inverter and the quality of the filter, a reduction in the rate of harmonic distortion can be observed. We can see that the profile of this voltage is closer to the sinusoid.

Figure 16 shows the regulation of the forward voltage after the three-phase two-phase transformation and the two-phase three-phase transformation. It can be seen that the current follows its reference and overshoot is not too noticeable. This shows good regulation using the PI controller from the PPL phase-locked loop.

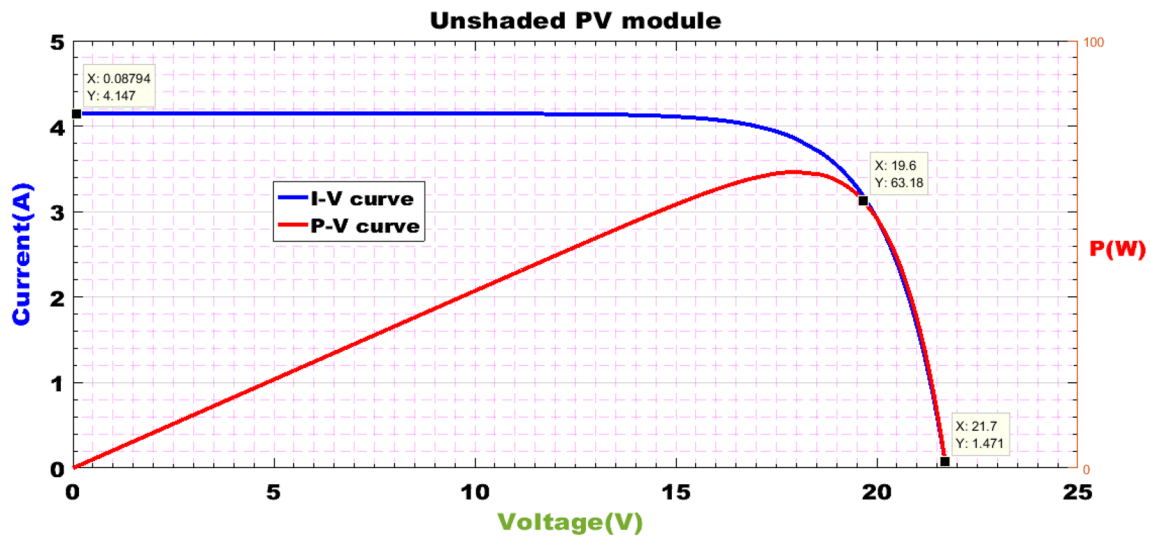


Fig. 18 I-V and P-V characteristics of PV module

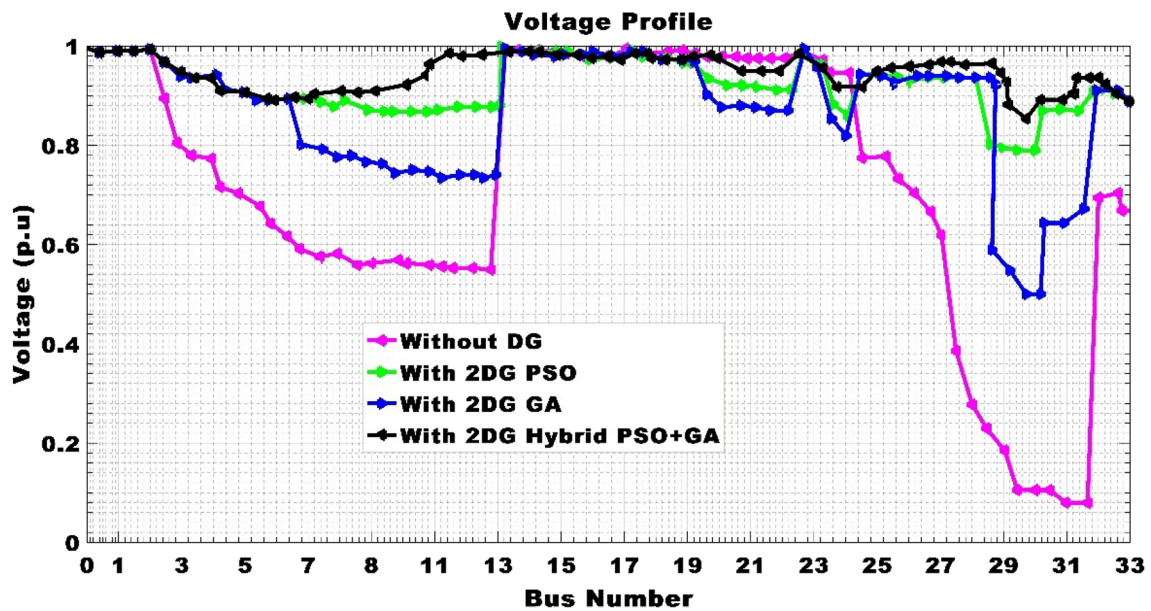


Fig. 19 Test using IEEE 33 bus

Figure 17 shows the power generated by the wind farm and its C_p coefficient on the same graph. It can be seen that the power has a good profile and a production of 2200 kW is observed for a maximum of C_{pmax} at 54%. This curve shows the power profile and the level reached by the C_p coefficient as a function of speed over a 24-h period.

Figure 18 shows the current voltage and power voltage characteristics. It can be seen that power is delivered under normal conditions. This will not be the same when the system is subjected to stochastic disturbances such

as variations in sunshine or temperature due to shading. This figure shows the power and current profile in the absence of total or partial shading.

Figure 19 shows the voltage profile of photovoltaic and wind energy sources. These voltage profiles are obtained by hybridizing the PSO algorithms with the algorithms. It can be seen that when the algorithms have improved performance, they are combined to manage the constraints and complexities of chaotic systems. In the absence of a combination of two primary sources, we find that the voltage profile is unstable

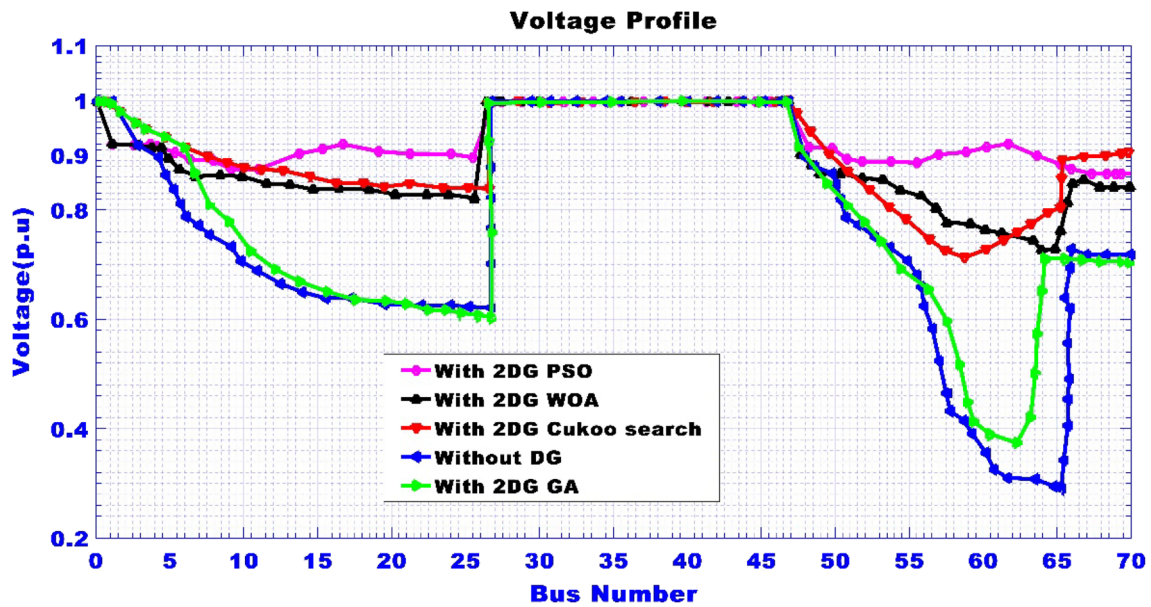


Fig. 20 Test using IEEE 69 bus

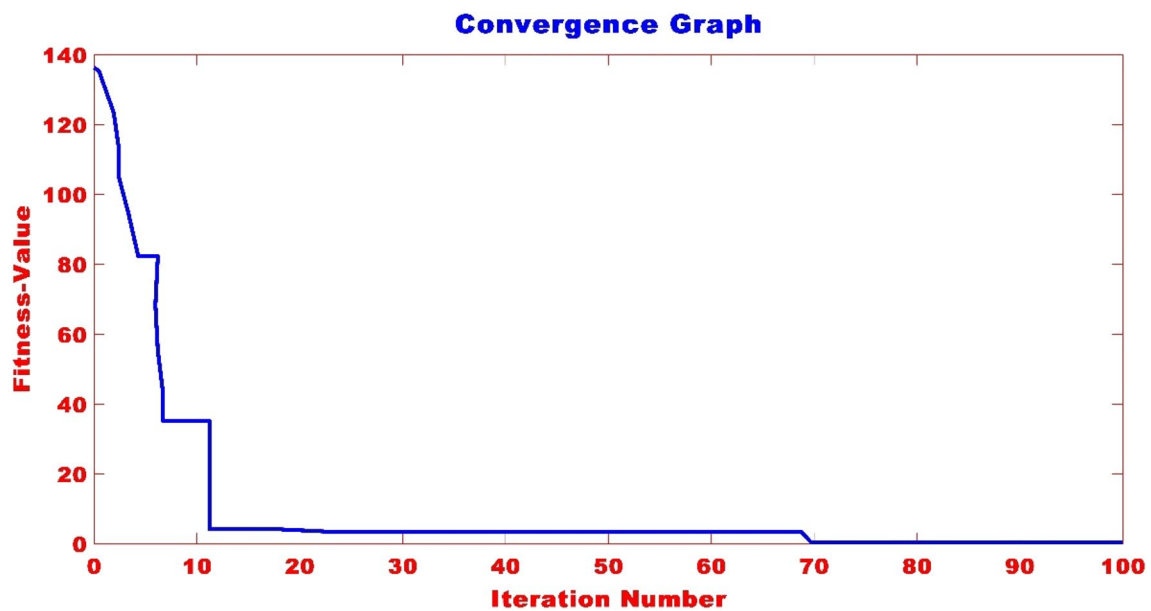


Fig. 21 Convergence of fitness function using PSO

whereas when we merge photovoltaic and wind sources, we have a good voltage profile. A bad voltage profile is when there is only one voltage source. The voltage level is unstable when only one source is used, whereas it is stable when the two sources are merged. The curve shows voltage stability when two sources are merged. This is observed at buses 15, 17, 19 and 24, where non-linear loads can be connected without creating network instability. For voltage level compensation in the event

of a deficit, the integration of a battery bank makes it possible to regulate these voltage dips.

Figure 20 shows the voltage profile of different configurations using the PSO, WOA, Cuckoo search and GA algorithms. In this section we are interested in observing the merging behavior of two renewable energy sources, commonly known as distributed generation (DG). For the present work, the two DGs are the photovoltaic source and the wind source. For this figure,

Table 3 Evaluation of power losses on IEEE 33 bus

Bus numbers	Distributed generations sizes (MW)	Plosses kW	Qlosses kVar
2	8.068	10.580	23.760
3	8.344	7.198	16.569
4	4.531	9.117	18.691
5	7.300	5.661	11.894
6	7.522	5.662	12.020
7	7.500	4.659	10.897
8	6.7758	5.157	11.930
9	6.996	5.243	12.208
10	5.028	6.993	13.124
11	5.693	6.192	13.618
12	5.600	6.339	13.948
13	5.773	6.771	14.206
14	6.486	4.639	10.018
15	6.565	4.432	10.937
16	6.195	4.710	10.880
17	6.535	4.367	10.430
18	5.930	4.258	10.728
19	5.276	4.788	10.882
20	4.188	5.701	13.300
21	4.434	6.939	14.584
22	3.214	7.594	16.576
23	3.127	7.705	16.838
24	5.783	5.687	11.739
25	4.968	6.990	14.698
26	3.110	7.178	17.749
27	5.773	6.993	13.124
28	6.486	6.192	13.618
29	6.565	6.339	13.948
30	6.195	6.771	14.206
31	6.535	4.639	10.018
32	5.930	4.432	10.937
33	5.276	4.710	10.880

the voltage profile is presented for its photovoltaic and wind hybrid sources. With a single distributed generation (DG), the voltage profile is low and unstable compared with that for which there is a combination of two distributed generations (2DG). It can be seen that different DGs can be allocated to buses 25, 30, 35, 41 and 50 without disturbing the system. This voltage profile shows that the system is stable between bus 26 and bus 58. However, the system is unstable on buses 10, 20, 55 and 65. This test is based on the IEEE 69-bus standard.

Figure 21 shows the speed of convergence of the cost function which evaluates the size of the whole system and the allocation of its secondary sources to the different configuration buses of the radial point system, since

the system configures on the non-radial interconnected network. We can see that the function converges towards the best scores for an iteration of $n = 10$. Convergence is total and reaches the minimum cost from iteration $n = 70$.

Table 3 shows the power level at the various nodes of the radially configured 33 bus. The size of the different distributed generations is given and the power losses are evaluated on the different buses. The same applies to reactive power losses on the same voltage profile of the standard 33 bus. An average power of 5 MW is observed on almost all the buses. These buses represent the network connection nodes. It is therefore possible to connect to these different location's sizes consuming an average of 5 MW. This capacity is sufficient for 24-h operation without any stability or blackout.

Figure 22 shows the variation in current voltage and power voltage characteristics for a photovoltaic system connected to the DC bus when some modules are subjected to partial shading. Shading of 55% gives a power of 33.12 W on a module. This corresponds to a voltage of 18.47 V and a current of 1.79 A.

Figure 23 shows the search for a point of maximum power using the MPPT algorithm based on PSO, GA, WOA and Cuckoo search. It can be seen that for a variation in rotation speed at angles 11 degrees 9 degrees 7 degrees, 3 degrees and minus 3 degrees, the maximum torque c_p is obtained. We note that for negative or positive variation of these coefficients, the maximum is always obtained and the curve describes a function which follows the law of variation of the non-linear loads.

When the loads are connected, Fig. 24 shows the profile of grid power, solar power, wind power and household demand. Over a 24-h period, demand peaks are observed at 7 am and 6 pm. These phenomena correspond to household needs. From 6 pm onwards, people start to return home from work.

Figure 25 shows the configuration of the different combinations of hybrid sources with battery. It can be seen that the PV-Wind-grid-Battery scenario can satisfy demand compared with the other scenarios. This voltage profile is presented on the IEEE 33-bus standard test, which corresponds to the architecture of the radial system of the North Cameroon interconnected network, especially in the Lokoro locality. This shows that the wind and photovoltaic energy resources at this site are sufficient to produce a large amount of capacity to reinforce the electricity networks in this area. This capacity can meet the needs of households and be injected into neighboring areas.

Figure 26 shows the result observed on the test bench. This figure shows the shape of the inverter voltage and

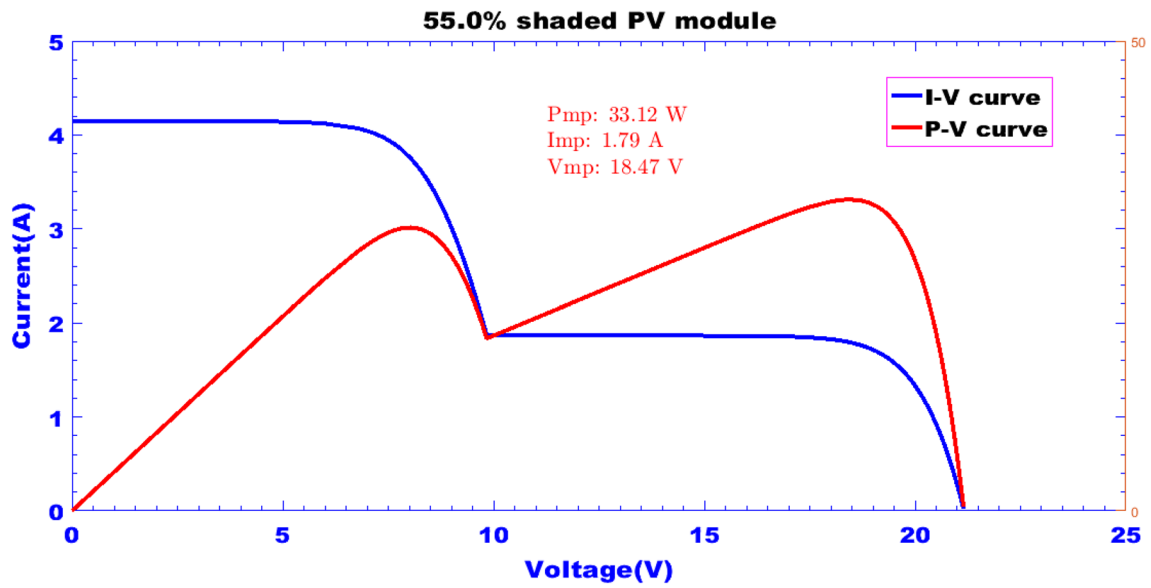


Fig. 22 I-V characteristics under partial shading of PV modules

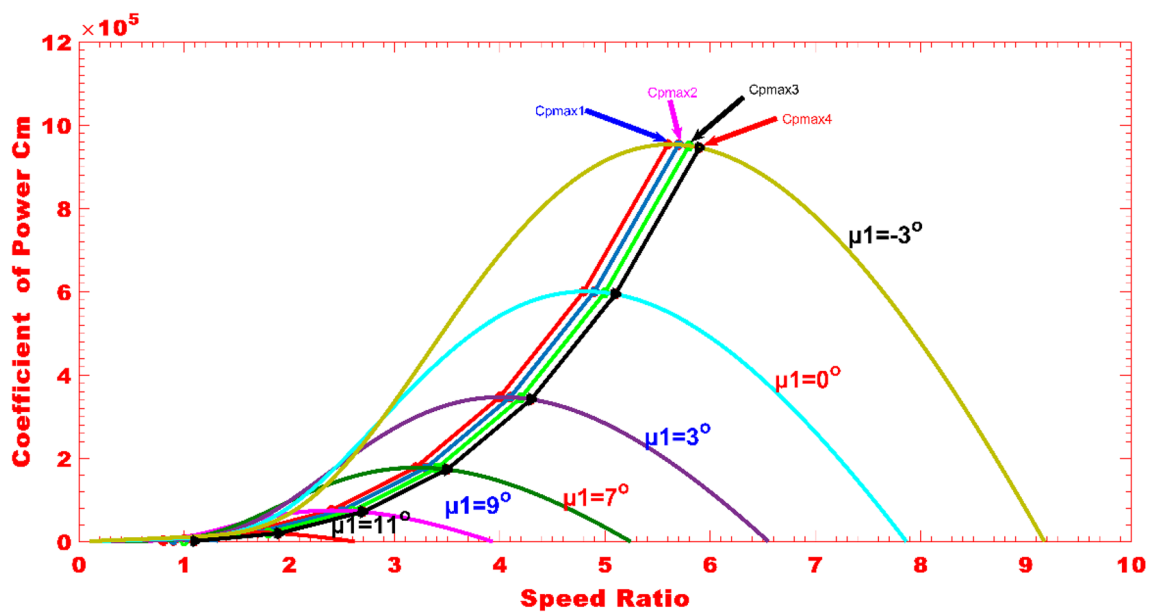


Fig. 23 Tracking MPP DFIG techniques

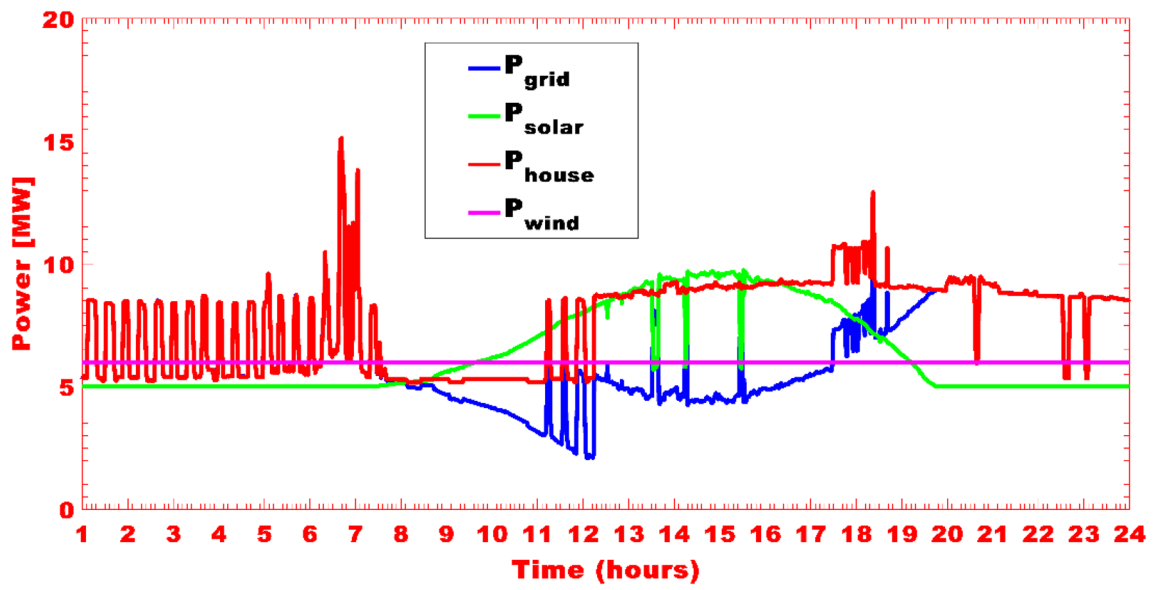


Fig. 24 Load Profiles considering overall system configuration

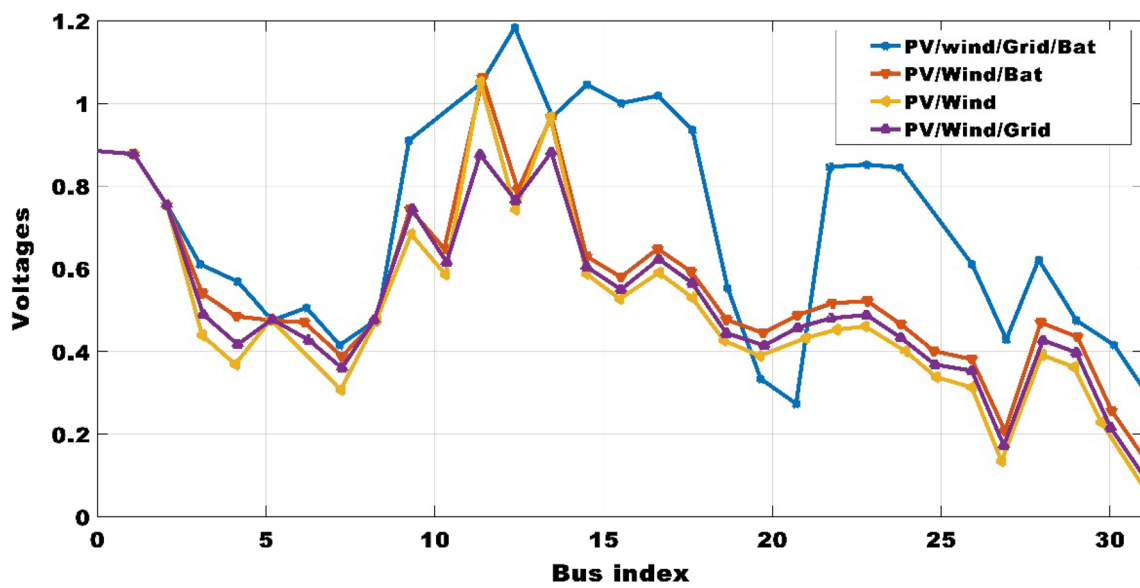


Fig. 25 Profile of Different proposed Scenarios

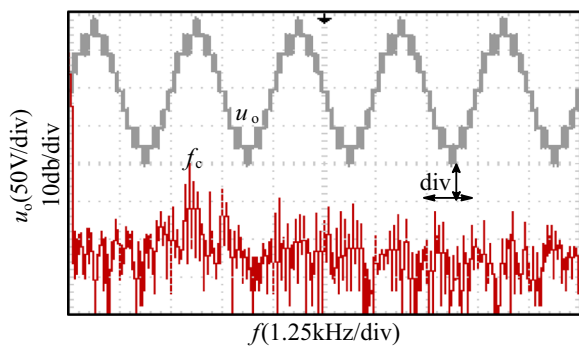


Fig. 26 Inverter under harmonics stresses and Frequency fluctuation

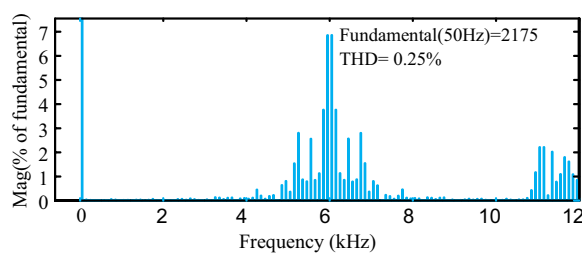


Fig. 27 Rate of total harmonic of distortion

the disturbance observed on the three three-phase lines. There are harmonic disturbances due to fluctuations and variations in frequency following peaks in demand from non-linear loads and shortfalls from primary sources (photovoltaic generator, wind power plant, battery discharges or network blackouts).

Figure 27 shows the rate of harmonic distortion for a 1958 kV fundamental amplitude at 50 Hz. The rate of harmonic distortion is obtained for $\text{THD} = 0.25\%$, which is much lower than the rate authorized for the integration of primary sources: photovoltaic and wind power, into an interconnected grid. This result complies with the connection standard and the norms in force. Evaluation of the harmonic distortion rate gives an idea of the quality of the energy and the voltage level observed at the common coupling point (CCP). We can see that the combination of these primary photovoltaic and wind sources does not produce too many network malfunctions, and that the filter has been able to clean up the distortions and pollution generated by the loads from households. This rate of harmonic distortion shows that the filter has played an important role on the one hand and that the size of the overall system has been well dimensioned on the other. This was achieved thanks to the PSO algorithms, which showed a good convergence speed for an iteration of less than $n = 10$. Thanks to these algorithms, the allocation or

connection of non-linear loads could be integrated into the various buses of the radial network. It can be seen that PSO algorithms combined with genetic algorithms are better suited to the allocation and sizing of distributed generation plants.

Conclusion

After evaluating the size of the entire photovoltaic-wind-battery-grid system using the PSO, WOA, GA and Cuckoo search algorithms, the technical and economic optimization was carried out in the software. The production cost of the system was observed at a discount for a 96% integration efficiency of the distributed generators. In other words, the algorithms were compared and analyzed. The PSO algorithms showed the best performance thanks to the convergence of the cost function. From data observed in HOMER and on the IEEE 33-bus and IEEE 69-bus test, it is reliable to carry out the configuration of the PV wind-battery-grid system to meet the demand at the locality of Lokoro, Cameroon. This system could not only meet the energy demand of the locality, but also compensate for the energy deficit in order to reinforce the North Cameroon interconnected grid. This proves that once the system is up and running, it will be possible to eliminate the load shedding and untimely power cuts that have been observed for more than five years in the northern part of Cameroon. In this part of the country, a number of localities and households have been unable to get electricity for three days out of every seven for almost five years. An assessment of the cost of the installation and the power loss will enable us to analyze the feasibility of the system and the impact of integrating it into the northern interconnected grid. However, this work could be limited because the parameters that currently influence the hydroelectric plant are not taken into account. There may be a shortage of water in the dam. This shortage can be seen as a prospect for meeting considerable demand and eliminating load shedding by reinforcing all the power lines in Cameroon.

Acknowledgements

The author acknowledges the department of Renewable Energy of National Advanced School of Engineering of Maroua, Cameroon for giving this chance to conduct this research. Authors are grateful to all friends for supporting their article.

Author contributions

B-PN: Conceptualization; Data curation; Formal analysis; Funding acquisition; Investigation; Methodology; NN: Project administration; Resources; Software; Validation; Visualization; Writing original draft. DKK: Conceptualization; Investigation; Methodology; Supervision; Writing original draft; Writing review and editing. ES: Formal analysis; Methodology; Supervision; Writing original draft. YBJ: Conceptualization; Investigation; Funding acquisition; Writing review and editing. SD: Methodology; Writing original draft; Writing review and editing.

K: Conceptualization; Data curation; Formal analysis; Writing original draft; Methodology; Supervision and editing.

Funding

No funding was declared.

Data Availability

Not applicable.

Declarations

Ethics approval and consent to participate

Not applicable.

Consent for publication

Not applicable.

Competing interests

The authors declare that they have no competing interests.

Author details

¹Department of Renewable Energy, University of Maroua, National Advanced School of Engineering of Maroua, P.O. Box 46, Maroua, Cameroon. ²Department of Computer Science and Telecommunications, University of Maroua, National Advanced School of Engineering of Maroua, P.O. Box 46, Maroua, Cameroon. ³Engineering, Koneru Lakshmaiah Education Foundation, Greenfields, Vaddeswaram, Guntur, Andhra Pradesh 522302, India. ⁴Bahir Dar Institute of Technology, Bahir Dar University, Bahir Dar, Ethiopia. ⁵Bengal College of Engineering and Technology, Durgapur, West Bengal 713212, India.

Received: 13 October 2022 Accepted: 24 August 2023

Published online: 15 September 2023

References

- Al-Ghussain, L., Ahmad, A. D., Abubaker, A. M., Abujubbeh, M., Almlaq, A., & Mohamed, M. A. (2021). A demand-supply matching-based approach for mapping renewable resources towards 100% renewable grids in 2050. *IEEE Access*, 9, 58634–58651. <https://doi.org/10.1109/ACCESS.2021.3072969>
- Alphonse, S., et al. (2011). Optimization PV/batteries system: Application in Wouro Kessoum Village Ngaoundere Cameroon. *Journal of Power and Energy Engineering*, 9(11), 50–59. <https://doi.org/10.4236/JPEE.2021.911003>
- Alturki, F. A., & Awwad, E. M. (2021). Sizing and cost minimization of stand-alone hybrid WT/PV/biomass/pump-hydro storage-based energy systems. *Energies*, 14(2), 489. <https://doi.org/10.3390/EN14020489>
- Amigue, F. F., Essiane, S. N., Ngoffe, S. P., Ondoa, G. A., Mengounou, G. M., & Nna Nna, P. T. (2021). Optimal integration of photovoltaic power into the electricity network using Slime mould algorithms: Application to the interconnected grid in North Cameroon. *Energy Reports*, 7, 6292–6307. <https://doi.org/10.1016/J.EGYR.2021.09.077>
- Bajaj, M., Welba, C., Bernard, K., Kamel, S., & El-Naggar, M. F. (2022). An experimental and case study on the evaluation of the partial shading impact on PV module performance operating under the Sudano-Sahelian Climate of Cameroon. *Frontiers in Energy Research*. <https://doi.org/10.3389/FENRG.2022.924285>
- Balan, G., et al. (2022). An improved deep learning-based technique for driver detection and driver assistance in electric vehicles with better performance. *International Transactions on Electrical Energy Systems*. <https://doi.org/10.1155/2022/8548172>
- Bello-Pierre, N., et al. (2023). Energy efficiency in periods of load shedding and detrimental effects of energy dependence in the City of Maroua, Cameroon. *Smart Grid Renewable Energy*, 14(4), 61–71. <https://doi.org/10.4236/SGRE.2023.144004>
- Come Zebra, E. I., van der Windt, H. J., Nhumai, G., & Faaij, A. P. C. (2021). A review of hybrid renewable energy systems in mini-grids for off-grid electrification in developing countries. *Renewable and Sustainable Energy Review*, 144, 111036. <https://doi.org/10.1016/J.RSER.2021.111036>
- Das, P., Das, B. K., Rahman, M., & Hassan, R. (2022). Evaluating the prospect of utilizing excess energy and creating employments from a hybrid energy system meeting electricity and freshwater demands using multi-objective evolutionary algorithms. *Energy*, 238, 121860. <https://doi.org/10.1016/J.ENERGY.2021.121860>
- De Oliveira, E. F., De Lima Tostes, M. E., De Freitas, C. A. O., & Leite, J. C. (2017). Voltage THD analysis using knowledge discovery in databases with a decision tree classifier. *IEEE Access*, 6, 1177–1188. <https://doi.org/10.1109/ACCESS.2017.2778028>
- Dieudonné, K. K., Bajaj, M., Rubanenko, O., Jurado, F., & Kamel, S. (2022). Hydropower potential assessment of four selected sites in the north interconnected network of Cameroon. *2022 IEEE Int. Conf. Autom. Congr. Chil. Assoc. Autom. Control Dev. Sustain. Agric. Syst. ICA-ACCA 2022*, <https://doi.org/10.1109/ICA-ACCA56767.2022.10005948>
- Djidimbélé, R., Ngoussandou, B.-P., Kidmo, D. K., Kitmo, Bajaj, M., & Raidandi, D. (2022). Optimal sizing of hybrid Systems for Power loss Reduction and Voltage improvement using PSO algorithm: Case study of Guissia Rural Grid. *Energy Reports*, 8, 86–95. <https://doi.org/10.1016/J.EGYR.2022.06.093>
- Donatus lweh, C., & Marius, L. (2019). Design of a hybrid wind-solar energy system for an agro-industrial residential area in Bota-Limbe, Cameroon. *Journal of Energy Power Engineering*, 13, 240–248. <https://doi.org/10.17265/1934-8975/2019.06.003>
- Garg, H. (2016). A hybrid PSO-GA algorithm for constrained optimization problems. *Applied Mathematics and Computation*, 274, 292–305. <https://doi.org/10.1016/J.AMC.2015.11.001>
- Gormo, V. G., Kidmo, D. K., Ngoussandou, B. P., Bogno, B., Raidandi, D., & Aillerie, M. (2021). Wind power as an alternative to sustain the energy needs in Garoua and Guider, North Region of Cameroon. *Energy Reports*, 7, 814–829. <https://doi.org/10.1016/J.EGYR.2021.07.059>
- Hermann, D. T., Donatien, N., Armel, T. K. F., & René, T. (2021). A feasibility study of an on-grid PV/Wind/Battery/Diesel for residential buildings under various climates in Cameroon. *Energy Technology*, 9(12), 2100615. <https://doi.org/10.1002/ENTE.202100615>
- Jaszczur, M., & Hassan, Q. (2020). An optimisation and sizing of photovoltaic system with supercapacitor for improving self-consumption. *Applied Energy*, 279, 115776. <https://doi.org/10.1016/j.apenergy.2020.115776>
- Jyothi, B., Bhavana, P., Rao, B. T., Pushkarna, M., Kitmo, A., & Djidimbele, R. (2023). Implementation of modified SEPIC converter for renewable energy built DC microgrids. *International Journal of Photoenergy*. <https://doi.org/10.1155/2023/2620367>
- Kavadias, K. A., & Triantafyllou, P. (2021). Hybrid renewable energy systems; optimisation. A review and extended comparison of the most-used software tools. *Energies*, 14(24), 8268. <https://doi.org/10.3390/EN14248268>
- Kebbati, Y., & Baghli, L. (2023). Design, modeling and control of a hybrid grid-connected photovoltaic-wind system for the region of Adrar, Algeria. *International Journal of Environmental Science and Technology*, 20(6), 6531–6558. <https://doi.org/10.1007/S13762-022-04426-Y/TABLES/6>
- Kidmo, D. K., Danwe, R., Doka, S. Y., Djongyang, N. (2015). Statistical analysis of wind speed distribution based on six Weibull Methods for wind power evaluation in Garoua, Cameroon. *Journal of Renewable Energies*, 18(1), 105–125–105–125. Accessed: Jan. 12, 2022. [Online]. Available: <https://revue.cder.dz/index.php/rer/article/view/491>
- Kitmo, Djidimbélé, R., Kidmo, D. K., Tchaya, G. B., & Djongyang, N. (2021). Optimization of the power flow of photovoltaic generators in electrical networks by MPPT algorithm and parallel active filters. *Energy Reports*, 7, 491–505. <https://doi.org/10.1016/J.EGYR.2021.07.103>
- Kitmo, Tchaya, G. B., & Djongyang, N. (2021). Optimization of the photovoltaic systems on the North Cameroon interconnected electrical grid. *International Journal of Energy and Environmental Engineering*, 13(1), 305–317. <https://doi.org/10.1007/S40095-021-00427-8>
- Kitmo, Tchaya, G. B., & Djongyang, N. (2022). Optimization of hybrid grid-tie wind solar power system for large-scale energy supply in Cameroon. *International Journal of Energy and Environmental Engineering*. <https://doi.org/10.1007/S40095-022-00548-8/METRICS>
- Li, Z., et al. (2020). Enhancing BCI-based emotion recognition using an improved particle swarm optimization for feature selection. *Sensors (Basel)*, 11(20), 3028. <https://doi.org/10.3390/s20113028>
- Lin, X. M., Kireeva, N., Timoshin, A. V., Naderipour, A., Abdul-Malek, Z., & Kamyab, H. (2021). A multi-criteria framework for designing of stand-alone and grid-connected photovoltaic, wind, battery clean energy system

- considering reliability and economic assessment. *Energy*, 224, 120154. <https://doi.org/10.1016/J.ENERGY.2021.120154>
- Lujano-Rojas, J. M., Dufo-López, R., & Bernal-Agustín, J. L. (2012). Optimal sizing of small wind/battery systems considering the DC bus voltage stability effect on energy capture, wind speed variability, and load uncertainty. *Applied Energy*, 93, 404–412. <https://doi.org/10.1016/J.APENERGY.2011.12.035>
- Ma, K., Soltani, M., Hajizadeh, A., Zhu, J., & Chen, Z. (2021). Wind farm power optimization and fault ride-through under inter-turn short-circuit fault. *Energies*. <https://doi.org/10.3390/EN14113072>
- Mahmoud, M. M., et al. (2022). Voltage quality enhancement of low-voltage smart distribution system using robust and optimized DVR controllers: Application of the Harris Hawks Algorithm. *International Transactions on Electrical Energy Systems*. <https://doi.org/10.1155/2022/4242996>
- Manjong, N. B., Oyewo, A. S., & Breyer, C. (2021). Setting the pace for a sustainable energy transition in central Africa: The case of Cameroon. *IEEE Access*, 9, 145435–145458. <https://doi.org/10.1109/ACCESS.2021.3121000>
- Meira Amaral da Luz, C., Roberto Ribeiro, E., & Lessa Tofoli, F. (2022). Analysis of the PV-to-PV architecture with a bidirectional Buck-Boost converter under shading conditions. *Solar Energy*, 232, 102–119. <https://doi.org/10.1016/J.SOLENER.2021.12.028>
- Mokhtara, C., Negrou, B., Settou, N., Settou, B., & Samy, M. M. (2021). Design optimization of off-grid Hybrid Renewable Energy Systems considering the effects of building energy performance and climate change: Case study of Algeria. *Energy*, 219, 119605. <https://doi.org/10.1016/J.ENERGY.2020.119605>
- Muh, E., Amara, S., & Tabet, F. (2018). Sustainable energy policies in Cameroon: A holistic overview. *Renewable and Sustainable Energy Reviews*, 82, 3420–3429. <https://doi.org/10.1016/J.RSER.2017.10.049>
- Njoh, A. J., Etta, S., Ngyah-Etchutambe, I. B., Enomah, L. E. D., Tabrey, H. T., & Essia, U. (2019). Opportunities and challenges to rural renewable energy projects in Africa: Lessons from the Esaghem Village, Cameroon solar electrification project. *Renewable Energy*, 131, 1013–1021. <https://doi.org/10.1016/J.RENENE.2018.07.092>
- Nsafon, B. E. K., Owolabi, A. B., Butu, H. M., Roh, J. W., Suh, D., & Huh, J. S. (2020). Optimization and sustainability analysis of PV/wind/diesel hybrid energy system for decentralized energy generation. *Energy Strategy Review*, 32, 100570. <https://doi.org/10.1016/j.esr.2020.100570>
- Olivares, D. E., Canizares, C. A., & Kazerani, M. (2014). A centralized energy management system for isolated microgrids. *IEEE Transaction Smart Grid*, 5(4), 1864–1875. <https://doi.org/10.1109/TSG.2013.2294187>
- Ram, M., Gulagi, A., Aghahosseini, A., Bogdanov, D., & Breyer, C. (2022). Energy transition in megacities towards 100% renewable energy: A case for Delhi. *Renewable Energy*, 195, 578–589. <https://doi.org/10.1016/J.RENENE.2022.06.073>
- Sawle, Y., Gupta, S. C., & Bohre, A. K. (2017). Optimal sizing of standalone PV/Wind/Biomass hybrid energy system using GA and PSO optimization technique. *Energy Procedia*, 117, 690–698. <https://doi.org/10.1016/J.EGYPRO.2017.05.183>
- Schulz, J., Leinmüller, D., Misik, A., & Zaeh, M. F. (2021). Renewable on-site power generation for manufacturing companies—technologies, modeling, and dimensioning. *Sustainability*, 13(7), 3898. <https://doi.org/10.3390/SU13073898>
- Shanmugam, Y., et al. (2022). A systematic review of dynamic wireless charging system for electric transportation. *IEEE Access*. <https://doi.org/10.1109/ACCESS.2022.3227217>
- Tamalouzt, S., Belkhier, Y., Sahri, Y., Bajaj, M., Ullah, N., Md. Chowdhury, S., Titsee-sang, T., & Techato, K. (2021). Enhanced direct reactive power control-based multi-level inverter for dfig wind system under variable speeds. *Sustainability*. <https://doi.org/10.3390/SU13169060>
- Tchaya, G. B., Kaoga, D. K., Alphonse, S., & Djongyang, N. (2021). Optimization of the smart grids connected using an improved P&O MPPT algorithm and parallel active filters. *Journal of Solar Energy Research*, 6(3), 814–828. <https://doi.org/10.22059/JSER.2021.320173.1196>
- Tonsie Djieba, R. H., Tiam Kapen, P., & Tchien, G. (2020). Wind energy of Cameroon by determining Weibull parameters: Potential of an environmentally friendly energy. *International Journal of Environmental Science and Technology*, 18(8), 2251–2270. <https://doi.org/10.1007/S13762-020-02962-Z>
- Varma, R. K., Rahman, S. A., Mahendra, A. C., Seethapathy, R., & Vanderheide, T. (2012). Novel nighttime application of PV solar farms as STATCOM (PV-STATCOM). *IEEE Power Energy Society General Meeting*. <https://doi.org/10.1109/PESGM.2012.6345657>
- Yaouba, Zieba Falama, R., Ngangoum Welaji, F., Hamda Soulouknga, M., Kwefeu Mbakop, F., & Dadjé, A. (2022). Optimal decision-making on hybrid off-grid energy systems for rural and remote areas electrification in the Northern Cameroon. *Journal of Electrical and Computer Engineering*. <https://doi.org/10.1155/2022/5316520>
- Zieba Falama, R., Kaoutoing, M. D., Mbakop, F. K., Dumbrava, V., Makloufi, S., Djongyang, N., Salah, C. B., & Doka, S. Y. (2022). A comparative study based on a techno-environmental-economic analysis of some hybrid grid-connected systems operating under electricity blackouts: A case study in Cameroon. *Energy Conversion and Management*, 251, 114935. <https://doi.org/10.1016/J.ENCONMAN.2021.114935>

Publisher's Note

Springer Nature remains neutral with regard to jurisdictional claims in published maps and institutional affiliations.

Submit your manuscript to a SpringerOpen® journal and benefit from:

- Convenient online submission
- Rigorous peer review
- Open access: articles freely available online
- High visibility within the field
- Retaining the copyright to your article

Submit your next manuscript at ► [springeropen.com](https://www.springeropen.com)